

Understanding and predicting extreme wildfires in the contiguous United States

Maxwell B. Joseph^{*1}, Matthew W. Rossi¹, Nathan P. Mietkiewicz¹, Adam L. Mahood¹, Megan E. Cattau¹, Lise Ann St. Denis¹, R. Chelsea Nagy¹, Virginia Iglesias¹, John T. Abatzoglou², and Jennifer K. Balch¹

¹Earth Lab, University of Colorado Boulder

²Department of Geography, University of Idaho

Abstract

Wildfires are becoming more frequent in parts of the globe, but predicting where and when extreme events occur remains difficult. To explain and predict wildfire extremes across the contiguous United States, we integrate a 30 year wildfire occurrence record with meteorological and housing data in spatiotemporal Bayesian models with spatially varying nonlinear effects. We compared models with different distributions for the number and sizes of large fires. A zero-inflated negative binomial model for fire counts and a lognormal model for burn areas provided the best performance. We find that dryness and air temperature strongly regulate wildfire risk, with precipitation, and housing density playing weaker roles. Statistically, most of the variability in the chance of an extreme wildfire results from changes in fire frequency that influence sampling from the tails of fire size distributions, rather than changes in the underlying distributions of expected fire sizes. Meteorologically, extreme events occur when conditions are hot and dry, but the effect of air temperature is spatially variable. This model attains 98.9% interval coverage for the number of fires in a withheld data set over a five-year prediction time horizon. We argue that recent wildfire extremes need not be surprising, and future extremes might be predictable if accurate meteorological forecasts are available to drive models of fire occurrence and size.

*maxwell.b.joseph@colorado.edu

1 Introduction

2 Wildfire frequency and burned area has increased over the past couple decades in the United
3 States (Dennison et al. 2014; Westerling 2016), and elsewhere (Krawchuk et al. 2009; Pechony
4 and Shindell 2010). In addition to the ecological and smoke impacts associated with increased
5 burned area, there has been an increasing interest in extreme wildfires (Williams 2013) given
6 their impact on human lives and infrastructure (Kochi et al. 2010; Diaz 2012). While case
7 studies of particular extremes provide insight into what caused past events (Peterson et al.
8 2015), predictions of future extremes at a national level could inform disaster related resource
9 allocation. Here, we consider an extreme wildfire to be a fire with the largest burned area
10 over a bounded spatiotemporal domain, e.g., within a spatial region and a temporal interval.

11 Factors driving wildfire extremes vary in space and time (Barbero et al. 2014), but it is
12 unclear how best to account for this in a predictive model. Previous efforts have used year or
13 region-specific models, aggregating over space or time (Bermudez et al. 2009), temporally or
14 spatially explicit models (Mendes et al. 2010), and spatial models with year as a covariate
15 (Díaz-Avalos, Juan, and Serra-Saurina 2016). Recently, rich spatiotemporal models have been
16 described with linear, spatially constant covariate effects (Serra, Saez, Juan, et al. 2014;
17 Serra, Saez, Mateu, et al. 2014). However, linear, spatially constant effects are suboptimal
18 over large spatial domains with nonlinear drivers (Fosberg 1978, Goodrick (2002), Preisler et
19 al. (2004); Preisler and Westerling 2007; Balshi et al. 2009; Krawchuk et al. 2009; Pechony
20 and Shindell 2009; Vilar et al. 2010; Woolford et al. 2011; Woolford et al. 2014). For
21 example, global wildfire probability shows a hump-shaped relationship with temperature and
22 moisture (Moritz et al. 2012). Interactions among drivers also impose nonlinearity, e.g., in
23 hot and dry climates fuel sparsity limits fire spread (McLaughlin and Bowers 1982), but in
24 cold and wet climates, fires are energy limited (Krawchuk and Moritz 2011).

25 Prediction is also complicated by uncertainty in which distribution(s) to use to assign
26 probabilities to extreme events. The generalized Pareto distribution (GPD) has frequently
27 been used (Bermudez et al. 2009; Jiang and Zhuang 2011), but the GPD requires a threshold
28 to delineate extreme events (Davison and Smith 1990, Coles (2014)). The utility and validity

29 of a threshold for extremes in a heterogeneous region is debatable (Tedim et al. 2018).
30 Recently proposed metastatistical extreme value (MEV) approaches do not require such a
31 threshold (Marani and Ignaccolo 2015; Zorzetto, Botter, and Marani 2016). In the MEV
32 framework, the occurrence and size of future events, and the parameters of their distributions
33 are treated as random variables which together imply a distribution for extremes. This
34 approach has roots in compound distributions (Dubey 1970; Wiitala 1999), doubly stochastic
35 processes (Cox and Isham 1980), superstatistics (Beck and Cohen 2003), and the Bayesian
36 posterior predictive distribution (Gelman et al. 2013). The link to Bayesian inference
37 is particularly useful, as it provides an easy way to propagate uncertainty forward to
38 predictions of extremes (Coles, Pericchi, and Sisson 2003).

39 Here, we extend the MEV perspective to account for non-linear, spatially varying wildfire
40 dynamics with the goal of predicting and explaining extreme wildfire events across the
41 contiguous United States. We aim to predict occurrence (where and when), and magnitude
42 (burn area) of large wildfires at a monthly time scale. Such predictions can be used to
43 prioritize reactive fire suppression resources or inform proactive wildfire risk mitigation.

44 **Methods**

45 **Data description**

46 We acquired wildfire event data for the contiguous United States from the Monitoring Trends
47 in Burn Severity (MTBS, www.mtbs.gov) program (Eidenshink et al. 2007), which includes
48 spatiotemporal information on the occurrence of wildfires in the United States from 1984 to
49 2015. The MTBS data contain fires greater than 1000 acres in the western U.S. and greater
50 than 500 acres in the eastern U.S. For consistency across the U.S., we discarded all records
51 in the MTBS data less than 1000 acres, retaining 10,315 fire events (Figure 1A). Each event
52 in the MTBS data has a discovery date, spatial point location, and final size.

53 To explain fire size and occurrence, we used a combination of meteorological variables
54 including humidity, air temperature, precipitation, and wind speed. These variables were

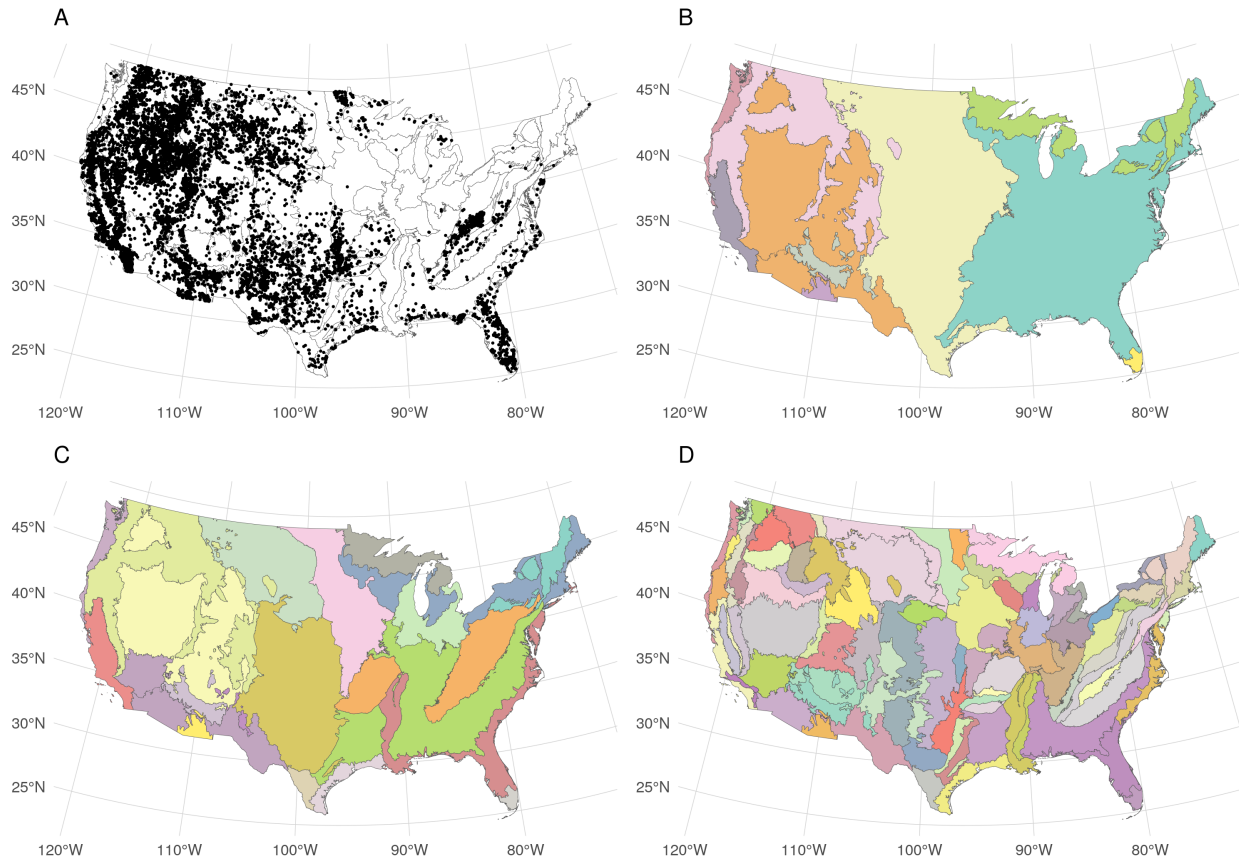


Figure 1. A. Fire ignition locations are shown as points across the study region. Colors in panels B, C, and D show level 1, 2, and 3 ecoregions respectively.

55 selected on the basis of previous work, and also with an aim to capture directly the effects
56 of easily interpretable meteorological quantities. Meteorological layers were acquired from
57 the gridMET data (Abatzoglou 2013) that blends monthly high-spatial resolution (~4-km)
58 climate data from the Parameter-elevation Relationships on Independent Slopes Model (Daly
59 et al. 2008) with high-temporal resolution (hourly) data from the National Land Data
60 Assimilation System (NLDAS2) using climatologically aided interpolation. The resultant
61 products are a suite of surface meteorological variables summarized at the daily time step
62 and at a 4-km pixel resolution. Daily total precipitation, minimum relative humidity, mean
63 wind speed, and maximum air temperature were averaged at a monthly time step for each of
64 84 Environmental Protection Agency level 3 (L3) ecoregions for each month from 1984 to
65 2015 (Omernik 1987; Omernik and Griffith 2014). We also computed cumulative monthly
66 precipitation over the previous 12 months for each ecoregion-month combination. We chose

67 to segment the U.S. with level 3 ecoregions as a compromise between the more numerous
68 (computationally demanding) level 4 ecoregions, and the coarser level 2 ecoregions.

69 We used publicly available housing density estimates that were generated based on the U.S.
70 2000 decennial census as explanatory variables that may relate to human ignition pressure
71 (Radeloff et al. 2010). These are provided at decadal time steps, and spatially at the level of
72 census partial block groups. To generate approximate measures of housing density at monthly
73 time intervals, we used a simple linear interpolation over time for each block group, then
74 aggregated spatially across block groups to compute mean housing density for each ecoregion
75 in each month.

76 **Model development**

77 We built two types of models: one describing the occurrence of fires within each L3 ecoregion
78 over time (i.e., the total number of fires occurring in each ecoregion for each month from
79 1984 - 2015), and another describing the size of each wildfire in each ecoregion and month.
80 For occurrence models, the response variable was a count (number of fires), and for burn
81 area models, the response was a continuous positive quantity (size of each fire event). We
82 used the period from 1984 to 2009 for training, withholding the period from 2010 to 2015 to
83 evaluate predictive performance.

84 **Fire occurrence**

85 We constructed four models for fire occurrence and compared their predictive performance
86 based on test-set log likelihood and posterior predictive checks for the proportion of zeros,
87 maximum count, and total count. The models differed in the distributions used in the
88 likelihood, representing counts as a Poisson, negative binomial, zero-inflated Poisson, or
89 zero-inflated negative binomial random variable. The Poisson distribution is a common choice
90 for counts, and the negative binomial distribution provides an alternative that can account
91 for overdispersion. The zero-inflated versions of these distributions include a component to
92 represent extra zeros, which might be expected to work well if there are independent processes

93 that determine whether nonzero counts are possible (Lambert 1992).

94 For spatial units (ecoregions) $s = 1, \dots, S$ and time steps (months) $t = 1, \dots, T$, each model
95 defines a probability mass function for $n_{s,t}$: the number of fires over 1000 acres in ecoregion
96 s and time step t . For each of the four count distributions under consideration, location
97 parameters $\mu_{s,t}$ and (for zero-inflated models) structural zero inflation parameters $\pi_{s,t}$ were
98 allowed to vary in space and time. We used a log link function to ensure that $\mu_{s,t} > 0$, and
99 a logit link function to ensure that $\pi_{s,t} \in (0, 1)$. Concatenating over spatial and temporal
100 units, so that $\boldsymbol{\mu} = (\mu_{s=1,t=1}, \mu_{s=2,t=1}, \dots, \mu_{s=S,t=1}, \mu_{s=S,t=2}, \dots, \mu_{s=S,t=T})$, and similarly for $\boldsymbol{\pi}$,
101 we modeled distributional location and (when applicable) zero inflation parameters as:

$$\log(\boldsymbol{\mu}) = \alpha^{(\mu)} + \mathbf{X}\boldsymbol{\beta}^{(\mu)} + \boldsymbol{\phi}^{(\mu)} + \log(\mathbf{a}),$$

$$\text{logit}(\boldsymbol{\pi}) = \alpha^{(\pi)} + \mathbf{X}\boldsymbol{\beta}^{(\pi)} + \boldsymbol{\phi}^{(\pi)},$$

102 where $\alpha^{(\mu)}$ and $\alpha^{(\pi)}$ are scalar intercept parameters, \mathbf{X} is a known $(S \times T) \times p$ design matrix,
103 where p is the number of input features, $\boldsymbol{\beta}^{(\mu)}$ and $\boldsymbol{\beta}^{(\pi)}$ are column vector parameters of length
104 p , $\boldsymbol{\phi}^{(\mu)}$ and $\boldsymbol{\phi}^{(\pi)}$ are column vector parameters of length $S \times T$ containing spatiotemporal
105 adjustments, and \mathbf{a} is a known offset vector of areas for spatial unit $s = 1, 2, \dots, S$, repeated
106 T times.

107 **Burn area**

108 We developed five candidate models for burn area, each of which specified a different
109 distribution for burn areas (Reed and McKelvey 2002; Hernandez et al. 2015), including the
110 generalized Pareto (Hosking and Wallis 1987), tapered Pareto (Schoenberg, Peng, and Woods
111 2003), lognormal, gamma, and Weibull distributions. We evaluated each model in terms of
112 test set log likelihood, and posterior predictive checks for burn area extremes. We defined
113 the response y_i as the number of acres burned over 1000 for the i^{th} fire event, which occurred
114 in spatial unit s_i and time step t_i .

115 Because each burn area distribution has a different parameterization, we included covariate ef-
116 fects in a distribution-specific way. For the generalized Pareto distribution (GPD), we assumed
117 a positive shape parameter, leading to a Lomax distribution for exceedances (Bermudez et al.
118 2009). The GPD and Lomax shape parameters are related by $\kappa^{(GPD)} = 1/\kappa^{(L)}$, and the GPD
119 scale parameter is related to the Lomax scale and shape parameters by $\sigma^{(GPD)} = \sigma^{(L)}/\kappa^{(L)}$.
120 We introduced covariate dependence via the Lomax scale parameter using a log link. For
121 event i , $\log(\sigma_i^{(L)}) = \alpha + \mathbf{X}_{(s_i, t_i)}\boldsymbol{\beta} + \phi_{s_i, t_i}$, where α is an intercept parameter, $\boldsymbol{\beta}$ is a length
122 p vector of coefficients, $\mathbf{X}_{(s_i, t_i)}$ is a row vector from \mathbf{X} , and ϕ_{s_i, t_i} is a spatiotemporal ad-
123 justment for s_i and t_i . For the tapered Pareto model, we modeled the shape parameter
124 as $\log(\kappa_i) = \alpha + \mathbf{X}_{(s_i, t_i)}\boldsymbol{\beta} + \phi_{s_i, t_i}$. The lognormal model included covariate dependence via
125 the location parameter: $\mu_i = \alpha + \mathbf{X}_{(s_i, t_i)}\boldsymbol{\beta} + \phi_{s_i, t_i}$. The gamma model used a log link for
126 the expected value: $\log(E(y_i)) = \alpha + \mathbf{X}_{(s_i, t_i)}\boldsymbol{\beta} + \phi_{s_i, t_i}$. Last, we modeled the Weibull scale
127 parameter as $\log(\sigma_i) = \alpha + \mathbf{X}_{(s_i, t_i)}\boldsymbol{\beta} + \phi_{s_i, t_i}$. More detail on the parameterization of each
128 burn area distribution is provided in the Supporting Information.

129 **Accounting for nonlinear forcing**

130 The design matrix \mathbf{X} was constructed to allow for spatially varying nonlinear effects of
131 housing density and meteorological drivers. We used B-splines to account for nonlinearity
132 (Figure 2) and allowed the coefficients for each basis vector to vary spatially (Wood 2017).
133 First, we constructed univariate B-splines for log housing density, wind speed, same month
134 precipitation, previous 12 month precipitation, air temperature, and humidity, with five
135 degrees of freedom (including an intercept) for each variable. This step generated 30 basis
136 vectors (five for each of six variables).

137 To allow for spatial variation in these nonlinear effects, we added interaction effects between
138 each of the basis vectors and ecoregions (Brezger and Lang 2006; Kneib, Hothorn, and Tutz
139 2009). The hierarchical nesting of ecoregion designations (Figure 1B-D) lends itself to such
140 interactions. Conceptually, coefficients in a level 3 ecoregion may be related to coefficients
141 in the level 2 ecoregion containing the level 3 region, the level 1 ecoregion containing the
142 level 2 region, and a global effect. The coefficient associated with a basis vector for any level

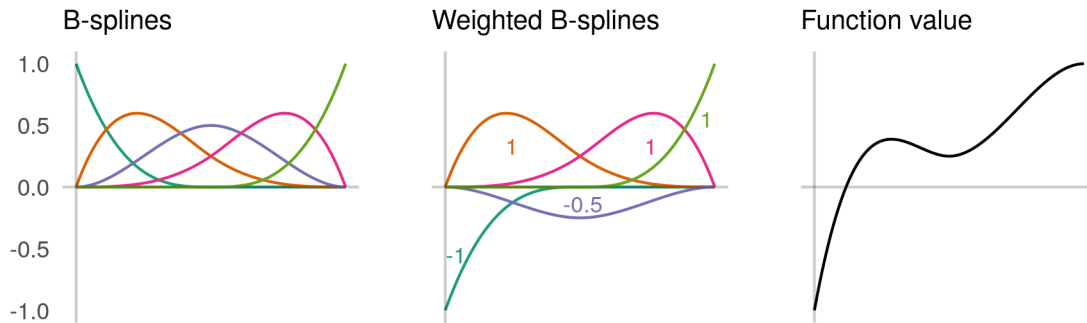


Figure 2. Conceptual figure to illustrate the use of B-splines to construct nonlinear functions. In the left panel, five B-spline vectors are shown, which map values of an input variable (on the x-axis) to a value on the y-axis. The middle panel shows the same B-spline vectors, but weighted (multiplied) by real numbers, with the weights illustrated as annotations. These weighted B-spline vectors are summed to produce the values of a nonlinear function (right panel).

143 3 ecoregion is treated as a sum of a global effect, a level 1 ecoregion adjustment, a level 2
144 ecoregion adjustment, and a level 3 ecoregion adjustment. Thus, for every univariate basis
145 vector, we included interaction effects with ecoregion at each of the three ecoregion levels.
146 This allows borrowing of information across space (level 3 ecoregions in a level 2 ecoregion are
147 often adjacent), and for regions that are ecologically similar. We also included adjustments
148 on the global intercept for each level 1, 2, and 3 ecoregion to account for spatial variation that
149 is unrelated to climate or housing density. This specification induces sparsity in \mathbf{X} that we
150 exploit to increase the efficiency of computing $\boldsymbol{\mu}$ and $\boldsymbol{\pi}$. In total, \mathbf{X} has $p = 3,472$ columns,
151 with 97% zero entries.

152 **Prior specification**

153 To avoid overfitting, we used a regularized horseshoe prior on the coefficients associated
154 with the spatially varying nonlinear effects described above (Piiironen, Vehtari, and others
155 2017). This prior places high probability close to zero, while retaining heavy enough tails
156 that nonzero coefficients are not shrunk too strongly toward zero. This is consistent with

157 our prior expectation that most of the coefficients associated with the columns in \mathbf{X} were
158 close to zero. For the zero inflated count models, we used a multivariate horseshoe to allow
159 information sharing between the zero inflated and distribution specific location parameters
160 (Peltola et al. 2014). For the remaining count models and all burn area models, this
161 was a univariate horseshoe prior. Spatiotemporal random effects were constructed using
162 a temporally autoregressive, spatially intrinsically autoregressive formulation (Besag and
163 Kooperberg 1995; Banerjee, Carlin, and Gelfand 2014). Details of these priors and the
164 resulting joint distributions are provided in the Supporting Information.

165 **Posterior predictive inference and extremes**

166 We used the posterior predictive distribution to check each model and make inference on
167 extremes. The posterior predictive distribution provides a distribution for replications of
168 observed data (y^{rep}), and predictions of future data (Gelman et al. 2013). Conceptually, for
169 a “good” model, y^{rep} should be similar to observed training data y , and future predictions
170 should be similar to future data. Distributions over both quantities can be obtained by
171 conditioning y and marginalizing over model parameters θ , e.g., $[y^{\text{rep}}|y] = \int [y^{\text{rep}}|\theta][\theta|y]d\theta$.

172 Posterior predictive distributions facilitate model checks that compare predicted and observed
173 test statistics (Gelman, Meng, and Stern 1996). To evaluate whether a model captures
174 tail behavior, one can compare an empirical maximum ($T(y) = \max(y)$) to the predicted
175 distribution of maxima $T(y^{\text{rep}})$. We also include predictive checks for the proportion of
176 zero counts, and totals for count and burn area models. Posterior predictive inference for
177 maxima is similar in spirit to the MEV approach. Both obtain a distribution over maxima
178 by marginalizing over unknowns including the number of events, size of each event, and
179 parameters of their distributions (Marani and Ignaccolo 2015). However, a Bayesian approach
180 explicitly conditions on the observed data to obtain a posterior distribution of parameters.
181 Seeing this connection is useful in the context of including priors and propagating uncertainty
182 to derived parameters, including total burn areas and probabilities of million acre wildfires.

183 **Parameter estimation**

184 We used a combination of variational approximations and Hamiltonian Monte Carlo methods
185 to sample from the posterior distributions of count and burn area models. A variational
186 approximation (Kucukelbir et al. 2015) was used for count models to quickly identify a
187 preferred model and avoid excessive multi-day model runs. Models were fit in the Stan
188 probabilistic programming language using the `rstan` package (Carpenter et al. 2016; Stan
189 Development Team 2018). The best performing count model and all burn area models were
190 fit using the No-U-Turn Sampler (Hoffman and Gelman 2014). We ran four chains for 1000
191 iterations each, and discarded the first 500 iterations as warmup. Convergence was assessed
192 using visual inspection of trace plots, with potential scale reduction statistic values $\hat{R} \geq 1.1$
193 as an indicator convergence failure (Brooks and Gelman 1998).

194 **Implementation**

195 All data processing, model fitting, and visualization were implemented with open source
196 software, primarily in the R programming language (R Core Team 2017), and wrapped in
197 a reproducible workflow via GNU Make and Docker (Stallman, McGrath, and Smith 2004;
198 Boettiger 2015). Data cleaning and transformation required the R packages `assertthat` (Wick-
199 ham 2017a), `lubridate` (Grolemund and Wickham 2011), `Matrix` (Bates and Maechler 2018),
200 `pbapply` (Solymos and Zawadzki 2018), `splines` (R Core Team 2018), `tidyverse` (Wickham
201 2017b), and `zoo` (Zeileis and Grothendieck 2005). Spatial data were processed with `raster`
202 (Hijmans 2017), `rgdal` (Bivand, Keitt, and Rowlingson 2018), `sf` (Pebesma 2018), and `spdep`
203 (Bivand and Piras 2015). Finally, we used `cowplot` (Wilke 2017), `ggrepel` (Slowikowski 2018),
204 `ggthemes` (Arnold 2018), `patchwork` (Pedersen 2017), and `RColorBrewer` (Neuwirth 2014) for
205 visualization. The manuscript was written in R Markdown (Allaire et al. 2018). Analyses
206 were run on an Amazon Web Services m5.2xlarge EC2 instance with four physical cores and
207 32 GB of RAM, and the whole workflow requires ≈ 72 hours. All code to reproduce the
208 analysis is available on GitHub at <https://github.com/mbjoseph/wildfire-extremes> (Joseph
209 2018).

Table 1. Performance of count models on the test set in descending order. Posterior means are provided with standard deviations in parentheses.

Model	Holdout log likelihood
ZI Negative binomial	-3068 (55)
Negative binomial	-3090 (60)
ZI Poisson	-3526 (71)
Poisson	-4194 (124)

210 Results

211 Wildfire occurrence

212 The zero-inflated negative binomial distribution performed best on the held-out test set
213 (Table 1), and was able to recover the proportion of zeros, count maxima, and count totals
214 in posterior predictive checks for both the training and test data (Figure 3). All of the
215 other count models that we considered exhibited lack of fit to at least one of these statistics
216 in posterior predictive checks. Hereafter, we report results from the zero-inflated negative
217 binomial model.

218 Minimum relative humidity and maximum air temperature had the strongest effects on both
219 the zero-inflation component and the expected value of the negative binomial component
220 (Figure 4, posterior median for ρ : 0.663, 95% credible interval (CI): 0.361 - 0.86). The
221 model uncovered unique effects of meteorological variables at level 1, 2, and 3 ecoregions
222 (Figure 5). For example, a positive interaction effect between the second air temperature
223 basis vector and the L1 Great Plains ecoregions indicates that the expected number of
224 wildfires in plains ecoregions with cold conditions is high relative to other ecoregions. The
225 Ozark/Ouachita-Appalachian forest and Ozark Highlands were also identified as having
226 region-specific temperature effects (Figure 5). Twelve month total precipitation also had
227 region specific effects in the Mississippi Alluvial and Southeast Coastal Plains ecoregion,
228 where it tended to reduce fire risk (Figure 5). In contrast, increasing cumulative twelve month
229 precipitation tended to increase risk in desert ecoregions (Figure 4). Housing density showed

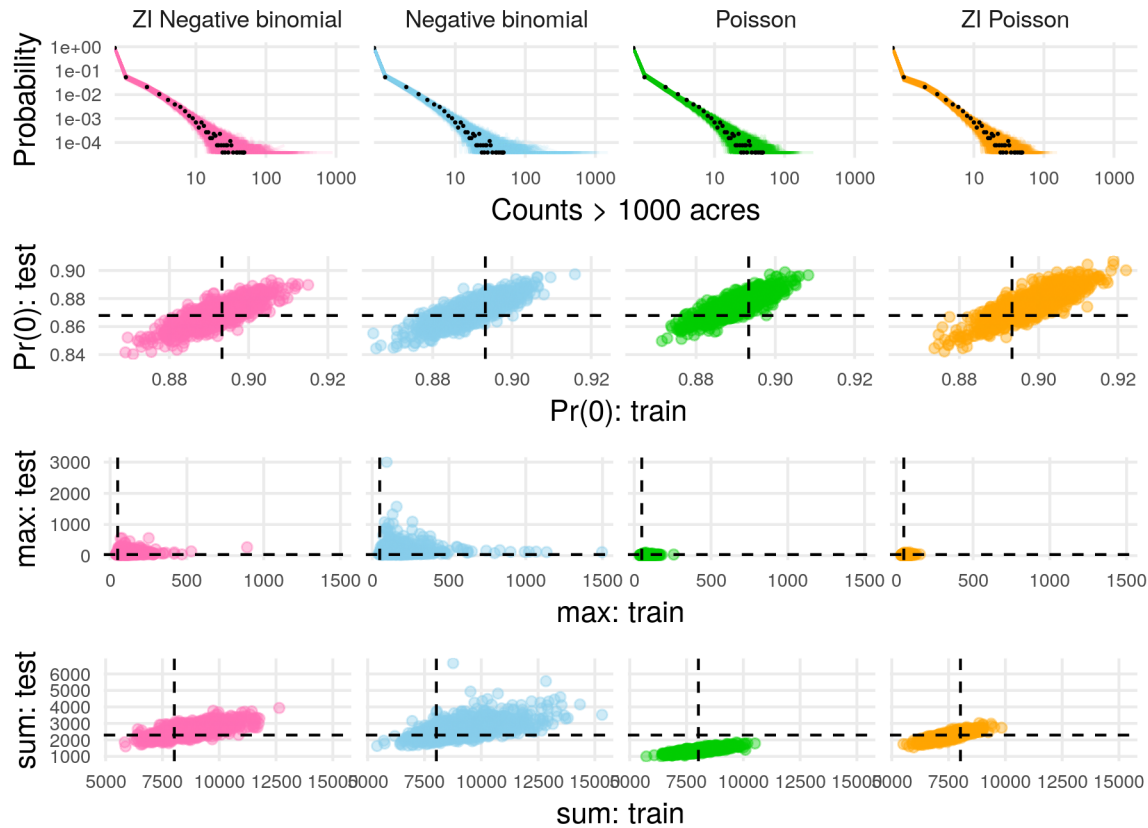


Figure 3. Count predictive checks. Row one shows observed count frequencies as black points and predicted frequencies as lines. Rows two, three, and four show predicted proportions of zeros, maxima, and sums (respectively) in the training and test data, with empirical values as dashed lines. Rows two through four facilitate comparison of performance on training and test sets. Ideally, model predictions cluster around the dashed lines for both the training (x-axis direction) and test (y-axis direction) sets, leading to a tight cluster of points at the intersection of the dashed lines.

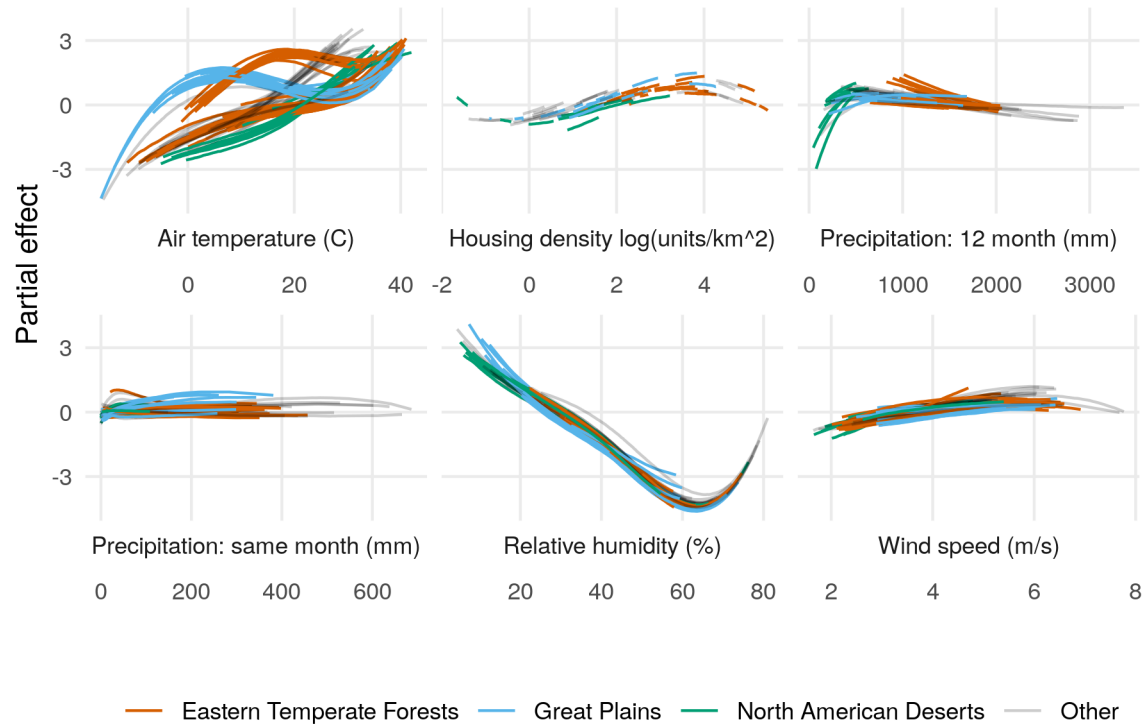


Figure 4. Partial effects on the log-transformed negative binomial mean component of the zero-inflated negative binomial model for each level 3 ecoregion, colored by level 1 ecoregion. Lines are posterior medians. Results are similar for the zero-inflation component.

230 a unimodal relationship to expected count (Figure 4), with lower expected counts in sparsely
231 populated ecoregions, and higher expected counts with moderately populated ecoregions.

232 Posterior 95% credible interval coverage for the number of fires over 1000 acres in the test
233 set was 98.9%. The lowest test set interval coverage was 91.7%, in the Cross Timbers L3
234 ecoregion. When observed counts fell outside the 95% prediction interval, counts were larger
235 than predicted 100% of the time. The largest difference between observed numbers and
236 predicted 97.5% posterior quantiles (the upper limit for the 95% credible interval) occurred
237 for the Columbia Mountains/Northern Rockies L3 ecoregion in August 2015, when 36 fires
238 over 1000 acres occurred and at most 23.025 were predicted. For nearly half of the level
239 3 ecoregions (44 of 85), accounting for 40.2% of the land area of the contiguous U.S., the
240 zero-inflated negative binomial model had 100% test set prediction interval coverage.

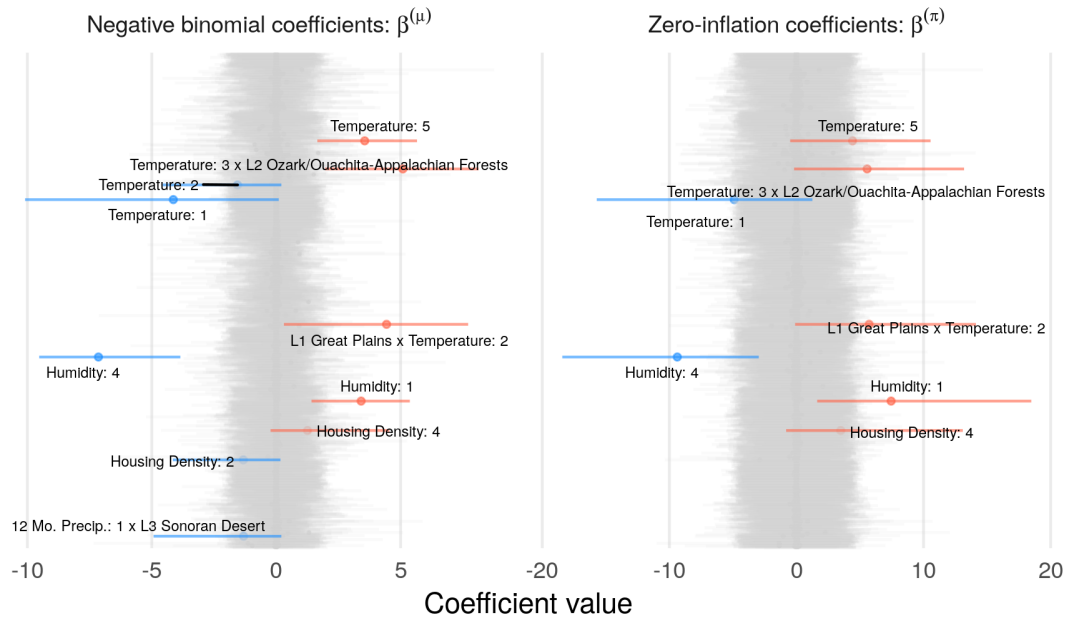


Figure 5. Caterpillar plots of zero inflated negative binomial model coefficients, $\beta^{(\mu)}$ (left) and $\beta^{(\pi)}$ (right). Horizontal line segments denote 95% credible intervals. Grey segments indicate coefficients with a less than 87% posterior probability of being positive or negative, and colored segments indicate coefficients that are probably positive (red) or negative (blue). B-spline vectors are indicated by colons, e.g., Humidity:1 indicates the first basis vector corresponding to humidity. Interactions between variables **a** and **b** are represented as Intxn(**a** x **b**). Level 1 ecoregions are represented by L1 ecoregion name, and L2 and L3 indicate level 2 and 3 ecoregions.

241 Wildfire burned areas

242 The lognormal distribution performed best on the test set (Table 2), and captured tail-
 243 behavior better than other burn area distributions (Figure 6). The GPD model was too
 244 heavy-tailed to adequately capture the pattern in the empirical data, predicting fires far
 245 larger than those observed in the training and test sets (Figure 6). The tapered Pareto
 246 distribution was too light-tailed (Figure 6). The gamma and Weibull models performed very
 247 poorly overall on the test set (Table 2), apparently due to a lack of congruence between the
 248 shapes of these distributions and the actual burn area distribution. Despite a poor fit to the
 249 bulk of the wildfire burn area distribution, both performed adequately in the upper tails

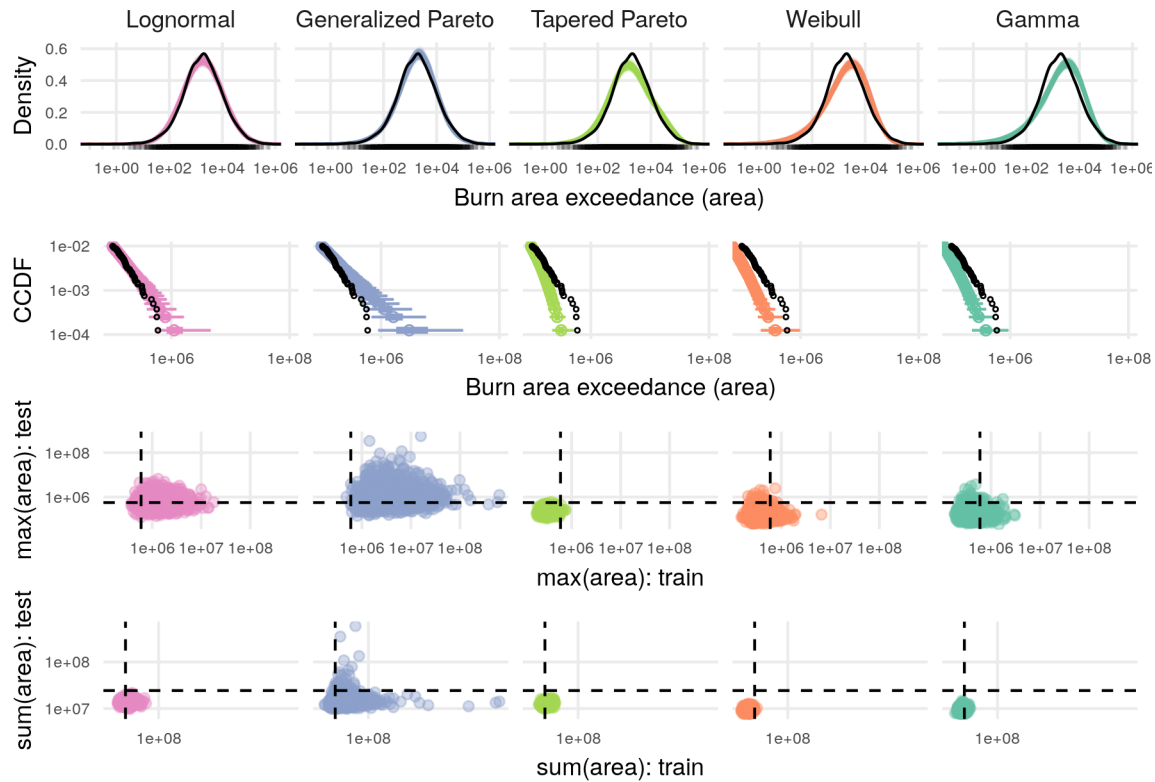


Figure 6. Predictive checks for burn area models. The top row shows predicted density in color and empirical density for the training set in black, which reveals overall lack of fit for the gamma and Weibull models. Row two shows the complementary cumulative distribution function (CCDF) at the tails, with 95% and 50% prediction intervals shown in color and observed data as black points, which shows that the Generalized Pareto distribution predicts values that are too extreme. The third and fourth rows show checks for maximum and total burn areas in the training and test set, with observed values as dashed lines and posterior draws as colored points. These final two rows facilitate checks for summary statistics on both the training and test set, with the ideal model generating predictions (colored points) clustered close to where the dashed lines intersect.

Table 2. Performance of burn area models on the test set in descending order. Posterior means are provided with standard deviations in parentheses.

Model	Holdout log likelihood
Lognormal	-22341 (39)
Generalized Pareto	-22375 (42)
Tapered Pareto	-22388 (48)
Weibull	-23499 (230)
Gamma	-26191 (908)

250 (Figure 6). Hereafter we present results for the lognormal model, which had the highest test
251 set log likelihood and captured tail behavior of the empirical fire size distribution.

252 Relative humidity was the primary driver of expected burn area for a fire event (Figure 7A).
253 The first basis vector for mean daily minimum relative humidity was the only coefficient with
254 a 95% credible interval that did not include zero (posterior median: 1.66, 95% CI: (0.57 -
255 2.28)). This nonlinear effect can be observed in Figure 7B as an increase in the expected burn
256 area below 20% mean daily minimum humidity. This leads to a seasonality gradient among
257 ecoregions of expected fire sizes, with little or no seasonal signal in typically humid ecoregions
258 such as Marine West Coast Forests of the Pacific Northwest, and seasonal oscillations in
259 ecoregions that have periodic fluctuations between dry and humid conditions such as the
260 Temperate Sierras (Figure 7C). There was not strong evidence that meteorological variables
261 had spatially variable effects on expected wildfire burn area.

262 Overall, 95% posterior predictive interval coverage in the test set for burn areas was 92.3%.
263 The lowest test set coverage was 0%, for the Eastern Great Lakes Lowlands L3 ecoregion,
264 followed by 50%, for the Central California Valley L3 ecoregion, though these ecoregions had
265 just 1 and 2 wildfire events in the test set. When observed fire sizes fell outside the 95%
266 prediction interval, 23.3% of wildfires were smaller than predicted, and 76.7% of wildfires
267 were larger than predicted. The largest discrepancy between the actual size of a wildfire and
268 the predicted 97.5% posterior quantile was observed with the Wallow Fire in 2011 which
269 burned 563,655 acres, but the predicted upper limit for size was 50,136. We investigate this

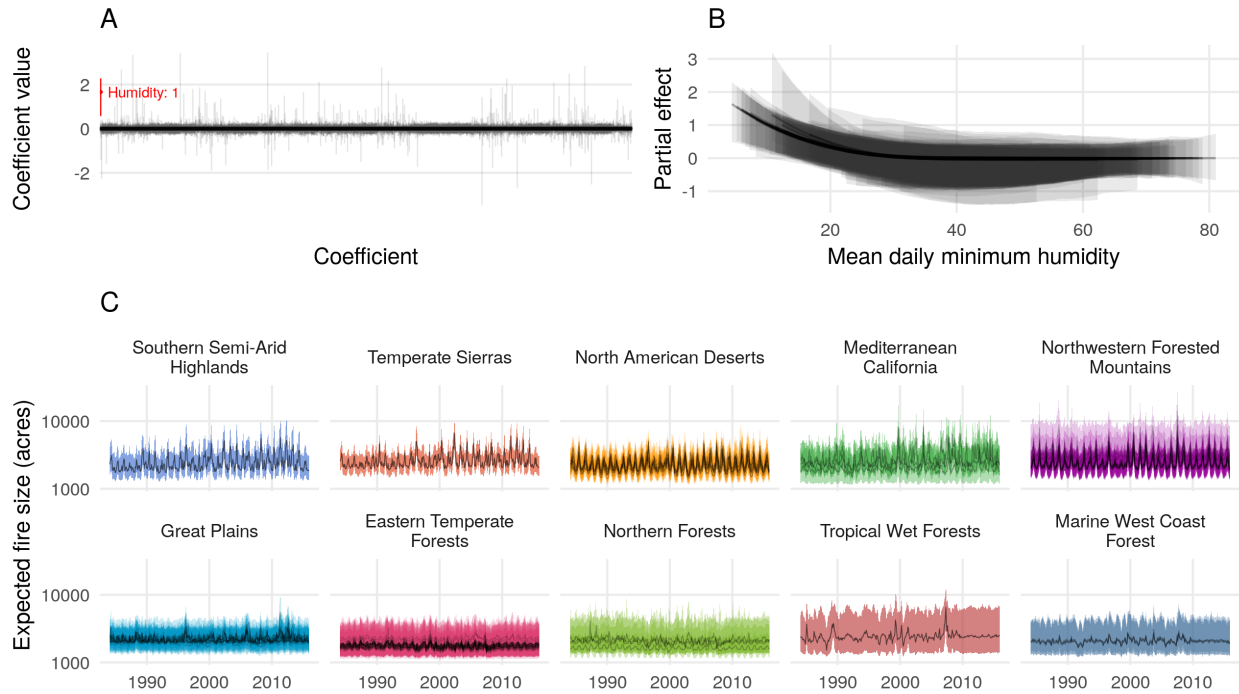


Figure 7. **A.** Estimated posterior medians and 95% credible intervals for each of the 3,473 coefficients associated with expected burn area. Only one coefficient - the first basis vector for humidity - had a 95% credible interval that excluded zero, shown in red. This effect is visualized in **B.** Partial effects of mean daily minimum humidity for each level 3 ecoregion, with posterior medians drawn as lines, and the 95% credible intervals as ribbons. **C.** Monthly time series of expected fire sizes for every level 3 ecoregion, faceted and colored by level 1 ecoregions sorted by mean humidity. Lines are posterior medians and ribbons are 95% credible intervals.

270 discrepancy further in the case study below. The lognormal burn area model achieved 100%
271 interval coverage in 26 of 66 ecoregions that had wildfire events in the test set, accounting
272 for 29% of the land area of the contiguous U.S.

273 Inference on extremes

274 By combining the output of the event count and burn area models, we derived posterior
275 prediction intervals for the size of the largest fire in a month for each region (the “burn area

276 maximum”), integrating over uncertainty in the number of fires, as well as the lognormal
277 mean and standard deviation for burn area. In the holdout period from 2010 to 2015, a 99%
278 prediction interval achieved 77.6% interval coverage, with 13.6% of the burn area maxima
279 (109 fire events) being larger than predicted (Figure 8). The model predicted the total area
280 burned over the entire contiguous United States in test period from 2010 to 2015 to be
281 28,407,396 (95% CI: (18,236,854 - 52,279,618) and the actual value was 26,639,835. While
282 fires over a million acres in size have happened historically, all fires in the training and
283 test sets were below one million acres. If we extrapolate, the probability that at least one
284 fire in the contiguous U.S. exceeded one million acres in the period from 2010 to 2015 was
285 estimated to be between 0.171 and 0.661 (95% CI), with a posterior median of 0.33. The
286 highest estimated probability for a million acre event was 0.014 (posterior median), with
287 a 95% CI of (0, 0.272) seen for the Southwestern Tablelands ecoregion in June 2011. The
288 second highest probability for a million acre event was 0.003 (posterior median), with a 95%
289 CI of (0, 0.048) seen for the Arizona/New Mexico Mountains ecoregion in June 2011.

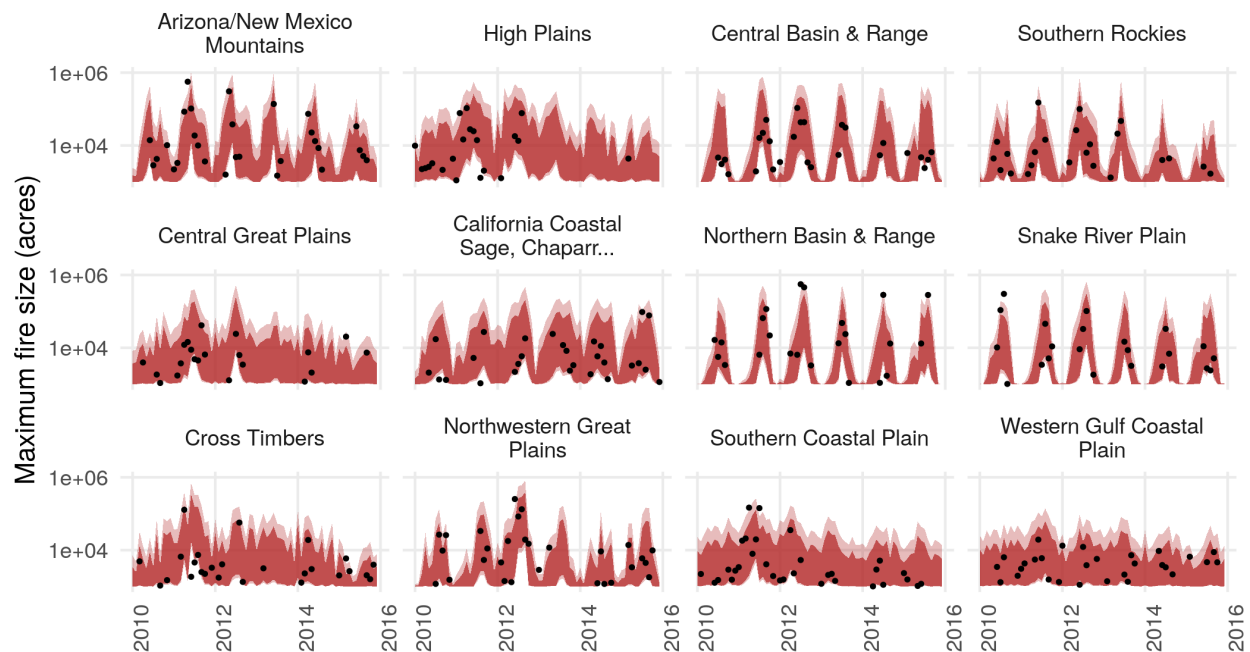


Figure 8. Posterior 99% (light red) and 95% (dark red) prediction intervals for the burn area of the largest fire event by month and level 3 ecoregion in the test set, shown for ecoregions with wildfires in more than 20 months. Empirical maxima are shown as black dots.

290 Error analysis case study: the 2011 Wallow Fire

291 To better understand how well the model could or could not anticipate notable extreme
292 events, and why, we used the largest fire in the test set as a case study. The Wallow Fire
293 was accidentally ignited on May 29, 2011 by two campers in the L3 Arizona/New Mexico
294 Mountains ecoregion. It burned through the month of June and into early July. The model
295 underpredicted the total burn area of the Wallow Fire. Integrating over uncertainty in the
296 predicted number of fires and expected fire size, the 99% credible interval for the maximum
297 fire size for May 2011 was (1,820 - 270,304) acres, but the Wallow Fire is recorded as 563,655
298 acres in the MTBS data.

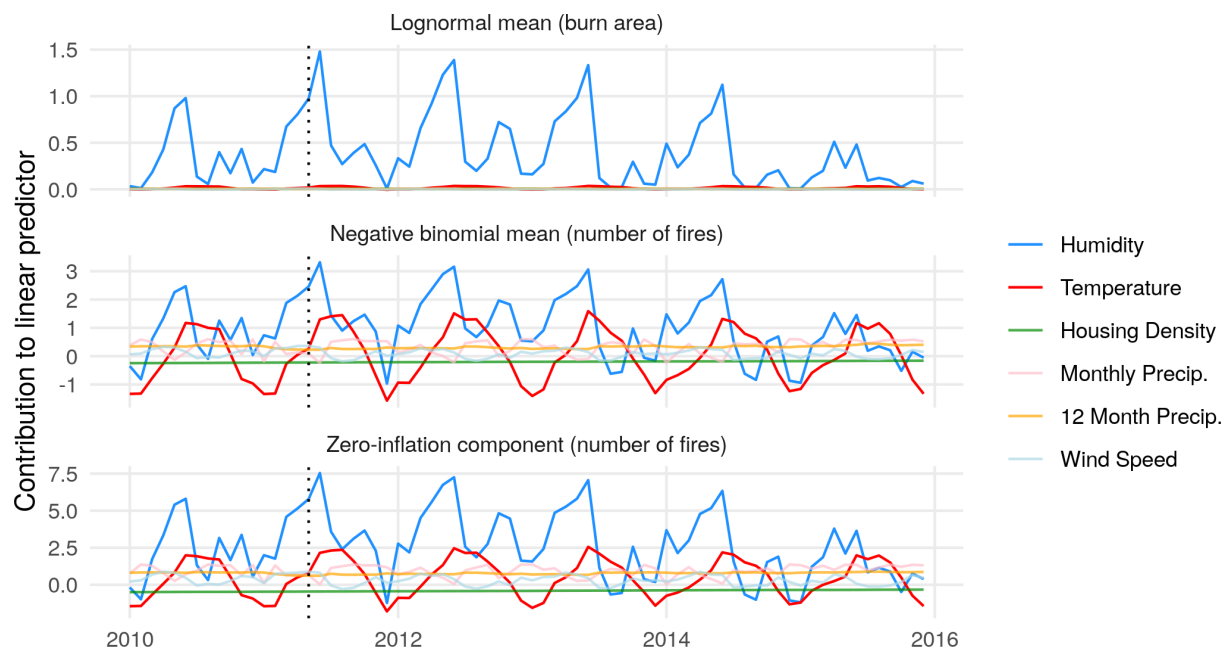


Figure 9. Posterior median contribution of each input variable to the linear predictor function of model components for the Arizona/New Mexico Mountains level 3 ecoregion from 2010-2016. A dotted vertical line marks May 2011, when the Wallow Fire ignited. Vertical positions of colored lines show contributions to the linear predictor function of each model component.

299 We evaluated the contribution of each covariate to the linear predictor functions of the three
300 model components (lognormal mean for burn areas, negative binomial mean for counts, and

301 the logit probability of the zero-inflation component) to understand why these predictions
302 differed. We defined the contribution of a variable as the dot product of the elements in
303 the design matrix \mathbf{X} corresponding to a particular driver variable (e.g., humidity), and the
304 estimated coefficients in β corresponding to that variable. This provides a quantitative
305 measure of how each input variable contributes to the linear predictor for an ecoregion, and
306 incorporates the overall, level 1, level 2, and level 3 ecoregion adjustments on these effects.
307 Humidity is the primary driver of variation in the model's predictions overall, and June 2011
308 - the month after ignition - favored more large fires, with drier, hotter conditions (Figure 9).
309 The 99% credible interval for June 2011 was (10,053 - 1,005,827) acres, which contains the
310 true value. Evidently, conditions in May that drove (under)predictions of maximum burn
311 area were not representative of the conditions over most of the Wallow Fire's duration. The
312 failure of the model to correctly predict the size of the Wallow fire suggests potential avenues
313 for improvement, discussed below.

314 Discussion

315 Extreme wildfires are often devastating, but perhaps they need not be surprising. By allowing
316 the non-linear effects of weather and housing density to vary across space, we were able to
317 achieve good predictive accuracy for fire extremes over a five-year prediction window. We
318 estimate a moderate chance of wildfires larger than what has been observed in recent decades,
319 perhaps even over one million acres. Such predictions can support short to medium term
320 wildfire management and probabilistic hazard assessment.

321 Driving a model with meteorological features raises challenges related to predictive uncertainty
322 and covariate shift - a change in the underlying distribution of forcing variables, potentially
323 outside of the historic range. Ideally, this uncertainty would be propagated forward in a
324 predictive model, possibly through stacking of predictive distributions that are generated from
325 multiple models of future climate dynamics (Yao et al. 2017). But, even if one had a perfect
326 forecast, novel conditions present a challenge for predictive modeling (Quionero-Candela et
327 al. 2009). For example, the High Plains ecoregion had its highest monthly precipitation,

328 lowest 12 month running precipitation, driest, hottest, and windiest conditions in the test set
329 period, so that the range of environmental conditions in the training data did not encompass
330 the range of future conditions. Extrapolating beyond the range of training inputs is generally
331 difficult, but the hierarchical spatial effect specification used here allows partial pooling
332 among climatically similar ecoregions that can inform such predictions, unlike models fit
333 separately to disjoint spatial regions.

334 Human-caused climate change is expected to increase fire activity in the western U.S. (Rogers
335 et al. 2011; Westerling et al. 2011; Moritz et al. 2012; Abatzoglou and Williams 2016)
336 and elsewhere (Flannigan et al. 2009), which when coupled with the nonlinear effect of
337 human-density provides a key inferential wrinkle. While most U.S. ecoregions are increasing
338 in human density over time, some of these ecoregions are in the range of values in which
339 this increases the expected number of large fires, while others are so populated that further
340 increases would reduce the chance of a large fire. The hump-shaped effect of human density
341 on the expected number of large fires is likely driven by ignition pressure and fire suppression
342 (Balch et al. 2017). As human density increases from zero, ignition pressure increases, but
343 eventually landscapes become so urbanized, fragmented, and/or fire-suppressed that wildfire
344 risk decreases (Syphard et al. 2007; Bowman et al. 2011; Bistinas et al. 2013; Knorr et al.
345 2013; Mcwethy et al. 2013; Syphard et al. 2017; Nagy et al. 2018). At intermediate density,
346 wildfire dynamics respond to human ignition and altered fuel distributions (Guyette, Muzika,
347 and Dey 2002), but these responses depend on environmental context and characteristics of
348 the human population (Marlon et al. 2008; Li et al. 2009). This model indicates that the
349 combination of moderate to high human density and dry conditions would nonlinearly increase
350 the chance of an extreme fire event. Both human density and dryness are expected to increase
351 in the future across large swaths of the U.S. (Lloyd, Sorichetta, and Tatem 2017; Stavros
352 et al. 2014, Radeloff et al. (2010)), with potential implications for human mortality, health
353 risks from smoke and particulate emission, and the financial burden of wildfire management
354 (Reid et al. 2016; Radeloff et al. 2018).

355 This work points to promising directions for future predictive efforts. Default choices such as
356 Poisson and GPD distributions should be checked against alternative distributions. Further,

357 the predictive skill of this model seems to suggest that ordinary events provide information on
358 extremes, which would not be the case if the generative distribution of extremes was completely
359 unique. Previous case studies have identified that extremes or anomalies in climatological
360 drivers play a role in the evolution of extreme wildfires (Peterson et al. 2015), but for this
361 work, monthly averages of climatological drivers over fairly large spatial regions were used,
362 which may smooth over anomalous or extreme conditions. Enhancing the spatiotemporal
363 resolution of predictive models could better represent climatic and social drivers of fire
364 dynamics and provide localized insights into fire dynamics to inform decision-making. This
365 raises computational challenges, but recent advances in distributed probabilistic computing
366 (Tran et al. 2017), efficient construction of spatiotemporal point processes (Shirota and
367 Banerjee 2018), and compact representations of nonlinear spatial interactions (Lee and
368 Durbán 2011) may provide solutions.

369 The Wallow Fire case study reveals at least one limitation of increasing the spatiotemporal
370 resolution. When the model predictions are driven by covariates that are summarized in space
371 and time (e.g. a mean across an ecoregion in a month), summary values may not represent
372 conditions that are most relevant to an event. With a discrete space-time segmentation,
373 events can occur at the boundary of a spatiotemporal unit, e.g., if a fire spreads into an
374 adjacent ecoregion or ignites on the last day of the month. Large wildfires can span months,
375 and a model that only uses conditions upon ignition to predict total burn area can fail to
376 account for conditions that change over the course of the event. Modeling ignitions as a point
377 process in continuous space and time (Brillinger, Preisler, and Benoit 2003), and explicitly
378 modeling subsequent fire duration and spatial dynamics could better separate conditions that
379 ignite fires from those that affect spread. Such an approach might be amenable to including
380 information on fuel continuity, which is likely to limit the size of extremely large fires and
381 did not factor into the current models predictions (Rollins, Morgan, and Swetnam 2002;
382 Hargrove et al. 2000). To the extent that a model reflects the generative process for extreme
383 events, the decomposition of contributions to the model's predictions may provide insight
384 into attribution for meteorological and anthropogenic drivers of extremes.

385 This paper presents and evaluates a statistical approach to explain and predict extreme

386 wildfires that incorporates spatially varying non-linear dynamics. The model reveals con-
387 siderable differences in fire dynamics among ecoregions spanning the mountain west to the
388 great plains, deserts, and eastern forests, and suggests a decent chance of very large fires
389 exceeding one million acres in the contiguous U.S. Predictive approaches such as this can
390 inform decision-making by placing probabilistic bounds on the number of wildfires and their
391 sizes, while provide deeper insights into wildfire ecology.

392 Acknowledgments

393 We thank Mitzi Morris, Kyle Foreman, Daniel Simpson, Bob Carpenter, and Andrew Gelman
394 for contributing to the implementation of an intrinsic autoregressive spatial prior in Stan.

References

Abatzoglou, John T. 2013. “Development of Gridded Surface Meteorological Data for Ecological Applications and Modelling.” *International Journal of Climatology* 33 (1). Wiley Online Library: 121–31.

Abatzoglou, John T., and A. Park Williams. 2016. “Impact of Anthropogenic Climate Change on Wildfire Across Western Us Forests.” *Proceedings of the National Academy of Sciences* 113 (42). National Academy of Sciences: 11770–5. doi:10.1073/pnas.1607171113.

Allaire, JJ, Yihui Xie, Jonathan McPherson, Javier Luraschi, Kevin Ushey, Aron Atkins, Hadley Wickham, Joe Cheng, and Winston Chang. 2018. *Rmarkdown: Dynamic Documents for R*. <https://CRAN.R-project.org/package=rmarkdown>.

Arnold, Jeffrey B. 2018. *Ggthemes: Extra Themes, Scales and Geoms for 'Ggplot2'*. <https://CRAN.R-project.org/package=ggthemes>.

Balch, Jennifer K, Bethany A Bradley, John T Abatzoglou, R Chelsea Nagy, Emily J Fusco, and Adam L Mahood. 2017. “Human-Started Wildfires Expand the Fire Niche Across the

United States.” *Proceedings of the National Academy of Sciences* 114 (11). National Acad Sciences: 2946–51.

Balshi, Michael S, A DAVID McGUIRE, Paul Duffy, Mike Flannigan, John Walsh, and Jerry Melillo. 2009. “Assessing the Response of Area Burned to Changing Climate in Western Boreal North America Using a Multivariate Adaptive Regression Splines (Mars) Approach.” *Global Change Biology* 15 (3). Wiley Online Library: 578–600.

Banerjee, Sudipto, Bradley P Carlin, and Alan E Gelfand. 2014. *Hierarchical Modeling and Analysis for Spatial Data*. CRC Press.

Barbero, R, JT Abatzoglou, EA Steel, and Narasimhan K Larkin. 2014. “Modeling Very Large-Fire Occurrences over the Continental United States from Weather and Climate Forcing.” *Environmental Research Letters* 9 (12). IOP Publishing: 124009.

Bates, Douglas, and Martin Maechler. 2018. *Matrix: Sparse and Dense Matrix Classes and Methods*. <https://CRAN.R-project.org/package=Matrix>.

Beck, Christian, and EGD Cohen. 2003. “Superstatistics.” *Physica A: Statistical Mechanics and Its Applications* 322. Elsevier: 267–75.

Bermudez, P de Zea, J Mendes, JMC Pereira, KF Turkman, and MJP Vasconcelos. 2009. “Spatial and Temporal Extremes of Wildfire Sizes in Portugal (1984–2004).” *International Journal of Wildland Fire* 18 (8). CSIRO Publishing: 983–91.

Besag, Julian, and Charles Kooperberg. 1995. “On Conditional and Intrinsic Autoregressions.” *Biometrika* 82 (4). Oxford University Press: 733–46.

Bistinas, Ioannis, Duarte Oom, Ana C. L. Sá, Sandy P. Harrison, I. Colin Prentice, and José M. C. Pereira. 2013. “Relationships between Human Population Density and Burned Area at Continental and Global Scales.” *PLoS ONE*. doi:10.1371/journal.pone.0081188.

Bivand, Roger, and Gianfranco Piras. 2015. “Comparing Implementations of Estimation Methods for Spatial Econometrics.” In. American Statistical Association.

Bivand, Roger, Tim Keitt, and Barry Rowlingson. 2018. *Rgdal: Bindings for the 'Geospatial'*

Data Abstraction Library. <https://CRAN.R-project.org/package=rgdal>.

Boettiger, Carl. 2015. “An Introduction to Docker for Reproducible Research.” *ACM SIGOPS Operating Systems Review* 49 (1). ACM: 71–79.

Bowman, David MJS, Jennifer Balch, Paulo Artaxo, William J Bond, Mark A Cochrane, Carla M D’antonio, Ruth DeFries, et al. 2011. “The Human Dimension of Fire Regimes on Earth.” *Journal of Biogeography* 38 (12). Wiley Online Library: 2223–36.

Brezger, Andreas, and Stefan Lang. 2006. “Generalized Structured Additive Regression Based on Bayesian P-Splines.” *Computational Statistics & Data Analysis* 50 (4). Elsevier: 967–91.

Brillinger, David R, Haiganoush K Preisler, and John W Benoit. 2003. “Risk Assessment: A Forest Fire Example.” *Lecture Notes-Monograph Series*. JSTOR, 177–96.

Brooks, Stephen P, and Andrew Gelman. 1998. “General Methods for Monitoring Convergence of Iterative Simulations.” *Journal of Computational and Graphical Statistics* 7 (4). Taylor & Francis: 434–55.

Carpenter, Bob, Andrew Gelman, Matt Hoffman, Daniel Lee, Ben Goodrich, Michael Betancourt, Michael A Brubaker, Jiqiang Guo, Peter Li, and Allen Riddell. 2016. “Stan: A Probabilistic Programming Language.” *Journal of Statistical Software* 20: 1–37.

Coles, S. 2014. *An Introduction to Statistical Modeling of Extreme Values*. Springer. <https://books.google.com/books?id=G-D-sgEACAAJ>.

Coles, Stuart, Luis Raúl Pericchi, and Scott Sisson. 2003. “A Fully Probabilistic Approach to Extreme Rainfall Modeling.” *Journal of Hydrology* 273 (1-4). Elsevier: 35–50.

Cox, David Roxbee, and Valerie Isham. 1980. *Point Processes*. Vol. 12. CRC Press.

Daly, Christopher, Michael Halbleib, Joseph I Smith, Wayne P Gibson, Matthew K Doggett, George H Taylor, Jan Curtis, and Phillip P Pasteris. 2008. “Physiographically Sensitive Mapping of Climatological Temperature and Precipitation Across the Conterminous United

States.” *International Journal of Climatology* 28 (15). Wiley Online Library: 2031–64.

Davison, Anthony C, and Richard L Smith. 1990. “Models for Exceedances over High Thresholds.” *Journal of the Royal Statistical Society. Series B (Methodological)*. JSTOR, 393–442.

Dennison, Philip E, Simon C Brewer, James D Arnold, and Max A Moritz. 2014. “Large Wildfire Trends in the Western United States, 1984–2011.” *Geophysical Research Letters* 41 (8). Wiley Online Library: 2928–33.

Diaz, John M. 2012. “Economic Impacts of Wildfire.” *Southern Fire Exchange*.

Díaz-Avalos, Carlos, Pablo Juan, and Laura Serra-Saurina. 2016. “Modeling Fire Size of Wildfires in Castellon (Spain), Using Spatiotemporal Marked Point Processes.” *Forest Ecology and Management* 381. Elsevier: 360–69.

Dubey, Satya D. 1970. “Compound Gamma, Beta and F Distributions.” *Metrika* 16 (1). Springer: 27–31.

Eidenshink, J, B Schwind, K Brewer, ZL Zhu, B Quayle, and S Howard. 2007. “A Project for Monitoring Trends in Burn Severity.” *Nutrition and Cancer* 58 (1): 28–34.

Flannigan, Mike D., Meg A. Krawchuk, William J. de Groot, B. Mike Wotton, and Lynn M. Gowman. 2009. “Implications of Changing Climate for Global Wildland Fire.” Journal Article. *International Journal of Wildland Fire* 18 (5): 483–507. doi:<http://dx.doi.org/10.1071/WF08187>.

Fosberg, Michael A. 1978. “Weather in Wildland Fire Management: The Fire Weather Index.” *US for Serv Reprints of Articles by FS Employees*.

Gelman, A., J.B. Carlin, H.S. Stern, D.B. Dunson, A. Vehtari, and D.B. Rubin. 2013. *Bayesian Data Analysis, Third Edition*. Chapman & Hall/Crc Texts in Statistical Science. Taylor & Francis. <https://books.google.com/books?id=ZXL6AQAAQBAJ>.

Gelman, Andrew, Xiao-Li Meng, and Hal Stern. 1996. “Posterior Predictive Assessment of

Model Fitness via Realized Discrepancies.” *Statistica Sinica*. JSTOR, 733–60.

Goodrick, Scott L. 2002. “Modification of the Fosberg Fire Weather Index to Include Drought.” *International Journal of Wildland Fire* 11 (4). CSIRO: 205–11.

Grolemund, Garrett, and Hadley Wickham. 2011. “Dates and Times Made Easy with lubridate.” *Journal of Statistical Software* 40 (3): 1–25. <http://www.jstatsoft.org/v40/i03/>.

Guyette, R. P., R. M Muzika, and D. C. Dey. 2002. “Dynamics of an Anthropogenic Fire Regime.” *Ecosystems* 5: 472–86. doi:10.1007/s10021-002-0115-7.

Hargrove, William W, RH Gardner, MG Turner, WH Romme, and DG Despain. 2000. “Simulating Fire Patterns in Heterogeneous Landscapes.” *Ecological Modelling* 135 (2-3). Elsevier: 243–63.

Hernandez, Charles, C Keribin, P Drobinski, and S Turquety. 2015. “Statistical Modelling of Wildfire Size and Intensity: A Step Toward Meteorological Forecasting of Summer Extreme Fire Risk.” In *Annales Geophysicae*, 33:1495–1506. 12.

Hijmans, Robert J. 2017. *Raster: Geographic Data Analysis and Modeling*. <https://CRAN.R-project.org/package=raster>.

Hoffman, Matthew D, and Andrew Gelman. 2014. “The No-U-Turn Sampler: Adaptively Setting Path Lengths in Hamiltonian Monte Carlo.” *Journal of Machine Learning Research* 15 (1): 1593–1623.

Hosking, Jonathan RM, and James R Wallis. 1987. “Parameter and Quantile Estimation for the Generalized Pareto Distribution.” *Technometrics* 29 (3). Taylor & Francis: 339–49.

Jiang, Yueyang, and Qianlai Zhuang. 2011. “Extreme Value Analysis of Wildfires in Canadian Boreal Forest Ecosystems.” *Canadian Journal of Forest Research* 41 (9). NRC Research Press: 1836–51.

Joseph, Max. 2018. “Mbjoseph/Wildfire-Extremes: First Release.” doi:10.5281/zenodo.1326858.

Kneib, Thomas, Torsten Hothorn, and Gerhard Tutz. 2009. “Variable Selection and Model

Choice in Geoadditive Regression Models.” *Biometrics* 65 (2). Wiley Online Library: 626–34.

Knorr, W, T Kaminski, A Arneth, and U Weber. 2013. “Impact of human population density on fire frequency at the global scale Impact of human population density on fire frequency at the global scale Impact of human population density on fire frequency at the global scale.” *Biogeosciences Discuss* 10: 15735–78. doi:10.5194/bgd-10-15735-2013.

Kochi, Ikuho, Geoffrey H Donovan, Patricia A Champ, and John B Loomis. 2010. “The Economic Cost of Adverse Health Effects from Wildfire-Smoke Exposure: A Review.” *International Journal of Wildland Fire* 19 (7). CSIRO: 803–17.

Krawchuk, Meg A, Max A Moritz, Marc-André Parisien, Jeff Van Dorn, and Katharine Hayhoe. 2009. “Global Pyrogeography: The Current and Future Distribution of Wildfire.” *PloS One* 4 (4). Public Library of Science: e5102.

Krawchuk, Meg A., and Max A. Moritz. 2011. “Constraints on global fire activity vary across a resource gradient.” *Ecology* 92 (1): 121–32. doi:10.1890/09-1843.1.

Kucukelbir, Alp, Rajesh Ranganath, Andrew Gelman, and David Blei. 2015. “Automatic Variational Inference in Stan.” In *Advances in Neural Information Processing Systems*, 568–76.

Lambert, Diane. 1992. “Zero-Inflated Poisson Regression, with an Application to Defects in Manufacturing.” *Technometrics* 34 (1). Taylor & Francis: 1–14.

Lee, Dae-Jin, and María Durbán. 2011. “P-Spline Anova-Type Interaction Models for Spatio-Temporal Smoothing.” *Statistical Modelling* 11 (1). SAGE Publications Sage India: New Delhi, India: 49–69.

Li, Li-Ming, Wei-Guo Song, Jian Ma, and Kohyu Satoh. 2009. “Artificial neural network approach for modeling the impact of population density and weather parameters on forest fire risk.” *International Journal of Wildland Fire* 18 (6). CSIRO PUBLISHING: 640. doi:10.1071/WF07136.

Lloyd, Christopher T, Alessandro Sorichetta, and Andrew J Tatem. 2017. “High Resolution Global Gridded Data for Use in Population Studies.” *Scientific Data* 4. Nature Publishing

Group: 170001.

Marani, Marco, and Massimiliano Ignaccolo. 2015. “A Metastatistical Approach to Rainfall Extremes.” *Advances in Water Resources* 79. Elsevier: 121–26.

Marlon, J. R., P. J. Bartlein, C. Carcaillet, D. G. Gavin, S. P. Harrison, P. E. Higuera, F. Joos, M. J. Power, and I. C. Prentice. 2008. “Climate and human influences on global biomass burning over the past two millennia.” *Nature Geoscience*. doi:10.1038/ngeo313.

McLaughlin, Steven P, and Janice E Bowers. 1982. “Effects of Wildfire on a Sonoran Desert Plant Community.” *Ecology*. JSTOR, 246–48.

Mcwethy, D. B., P. E. Higuera, C. Whitlock, T. T. Veblen, D. M J S Bowman, G. J. Cary, S. G. Haberle, et al. 2013. “A conceptual framework for predicting temperate ecosystem sensitivity to human impacts on fire regimes.” *Global Ecology and Biogeography* 22 (8): 900–912.

Mendes, Jorge M, Patrícia Cortés de Zea Bermudez, José Pereira, KF Turkman, and MJP Vasconcelos. 2010. “Spatial Extremes of Wildfire Sizes: Bayesian Hierarchical Models for Extremes.” *Environmental and Ecological Statistics* 17 (1). Springer: 1–28.

Moritz, Max A, Marc-André Parisien, Enric Batllori, Meg A Krawchuk, Jeff Van Dorn, David J Ganz, and Katharine Hayhoe. 2012. “Climate Change and Disruptions to Global Fire Activity.” *Ecosphere* 3 (6). Wiley Online Library: 1–22.

Nagy, R, Emily Fusco, Bethany Bradley, John T Abatzoglou, and Jennifer Balch. 2018. “Human-Related Ignitions Increase the Number of Large Wildfires Across Us Ecoregions.” *Fire* 1 (1). Multidisciplinary Digital Publishing Institute: 4.

Neuwirth, Erich. 2014. *RColorBrewer: ColorBrewer Palettes*. <https://CRAN.R-project.org/package=RColorBrewer>.

Omernik, James M. 1987. “Ecoregions of the Conterminous United States.” *Annals of the Association of American Geographers* 77 (1). Taylor & Francis: 118–25.

Omernik, James M, and Glenn E Griffith. 2014. “Ecoregions of the Conterminous United States: Evolution of a Hierarchical Spatial Framework.” *Environmental Management* 54 (6).

Springer: 1249–66.

Pebesma, Edzer. 2018. *Sf: Simple Features for R*. <https://CRAN.R-project.org/package=sf>.

Pechony, O, and DT Shindell. 2009. “Fire Parameterization on a Global Scale.” *Journal of Geophysical Research: Atmospheres* 114 (D16). Wiley Online Library.

Pechony, Olga, and Drew T Shindell. 2010. “Driving Forces of Global Wildfires over the Past Millennium and the Forthcoming Century.” *Proceedings of the National Academy of Sciences* 107 (45). National Acad Sciences: 19167–70.

Pedersen, Thomas Lin. 2017. *Patchwork: The Composer of Ggplots*. <https://github.com/thomasp85/patchwork>.

Peltola, Tomi, Aki S Havulinna, Veikko Salomaa, and Aki Vehtari. 2014. “Hierarchical Bayesian Survival Analysis and Projective Covariate Selection in Cardiovascular Event Risk Prediction.” In *Proceedings of the Eleventh Uai Conference on Bayesian Modeling Applications Workshop-Volume 1218*, 79–88. CEUR-WS. org.

Peterson, David A, Edward J Hyer, James R Campbell, Michael D Fromm, Johnathan W Hair, Carolyn F Butler, and Marta A Fenn. 2015. “The 2013 Rim Fire: Implications for Predicting Extreme Fire Spread, Pyroconvection, and Smoke Emissions.” *Bulletin of the American Meteorological Society* 96 (2): 229–47.

Piironen, Juho, Aki Vehtari, and others. 2017. “Sparsity Information and Regularization in the Horseshoe and Other Shrinkage Priors.” *Electronic Journal of Statistics* 11 (2). The Institute of Mathematical Statistics; the Bernoulli Society: 5018–51.

Preisler, Haiganoush K, and Anthony L Westerling. 2007. “Statistical Model for Forecasting Monthly Large Wildfire Events in Western United States.” *Journal of Applied Meteorology and Climatology* 46 (7): 1020–30.

Preisler, Haiganoush K, David R Brillinger, Robert E Burgan, and JW Benoit. 2004. “Probability Based Models for Estimation of Wildfire Risk.” *International Journal of Wildland Fire* 13 (2). CSIRO: 133–42.

Quionero-Candela, Joaquin, Masashi Sugiyama, Anton Schwaighofer, and Neil D Lawrence.

2009. *Dataset Shift in Machine Learning*. The MIT Press.

R Core Team. 2017. *R: A Language and Environment for Statistical Computing*. Vienna, Austria: R Foundation for Statistical Computing. <https://www.R-project.org/>.

———. 2018. *R: A Language and Environment for Statistical Computing*. Vienna, Austria: R Foundation for Statistical Computing. <https://www.R-project.org/>.

Radeloff, Volker C, David P Helmers, H Anu Kramer, Miranda H Mockrin, Patricia M Alexandre, Avi Bar-Massada, Van Butsic, et al. 2018. “Rapid Growth of the Us Wildland-Urban Interface Raises Wildfire Risk.” *Proceedings of the National Academy of Sciences* 115 (13). National Acad Sciences: 3314–9.

Radeloff, Volker C, Susan I Stewart, Todd J Hawbaker, Urs Gimmi, Anna M Pidgeon, Curtis H Flather, Roger B Hammer, and David P Helmers. 2010. “Housing Growth in and Near United States Protected Areas Limits Their Conservation Value.” *Proceedings of the National Academy of Sciences* 107 (2). National Acad Sciences: 940–45.

Reed, William J, and Kevin S McKelvey. 2002. “Power-Law Behaviour and Parametric Models for the Size-Distribution of Forest Fires.” *Ecological Modelling* 150 (3). Elsevier: 239–54.

Reid, Colleen E, Michael Brauer, Fay H Johnston, Michael Jerrett, John R Balmes, and Catherine T Elliott. 2016. “Critical Review of Health Impacts of Wildfire Smoke Exposure.” *Environmental Health Perspectives* 124 (9). National Institute of Environmental Health Science: 1334.

Rogers, Brendan M., Ronald P. Neilson, Ray Drapek, James M. Lenihan, John R. Wells, Dominique Bachelet, and Beverly E. Law. 2011. “Impacts of Climate Change on Fire Regimes and Carbon Stocks of the U.S. Pacific Northwest.” *Journal of Geophysical Research: Biogeosciences* 116 (G3): n/a–n/a. doi:10.1029/2011JG001695.

Rollins, Matthew G, Penelope Morgan, and Thomas Swetnam. 2002. “Landscape-Scale Controls over 20th Century Fire Occurrence in Two Large Rocky Mountain (Usa) Wilderness

Areas.” *Landscape Ecology* 17 (6). Springer: 539–57.

Schoenberg, Frederic Paik, Roger Peng, and James Woods. 2003. “On the Distribution of Wildfire Sizes.” *Environmetrics* 14 (6). Wiley Online Library: 583–92.

Serra, Laura, Marc Saez, Pablo Juan, Diego Varga, and Jorge Mateu. 2014. “A Spatio-Temporal Poisson Hurdle Point Process to Model Wildfires.” *Stochastic Environmental Research and Risk Assessment* 28 (7). Springer: 1671–84.

Serra, Laura, Marc Saez, Jorge Mateu, Diego Varga, Pablo Juan, Carlos Díaz-Ávalos, and Håvard Rue. 2014. “Spatio-Temporal Log-Gaussian Cox Processes for Modelling Wildfire Occurrence: The Case of Catalonia, 1994–2008.” *Environmental and Ecological Statistics* 21 (3). Springer: 531–63.

Shirota, Shinichiro, and Sudipto Banerjee. 2018. “Scalable Inference for Space-Time Gaussian Cox Processes.” *arXiv Preprint arXiv:1802.06151*.

Slowikowski, Kamil. 2018. *Ggrepel: Automatically Position Non-Overlapping Text Labels with 'Ggplot2'*. <https://CRAN.R-project.org/package=ggrepel>.

Solymos, Peter, and Zygmunt Zawadzki. 2018. *Pbapply: Adding Progress Bar to '*Apply' Functions*. <https://CRAN.R-project.org/package=pbapply>.

Stallman, Richard M., Roland McGrath, and Paul D. Smith. 2004. *GNU Make: A Program for Directing Recompilation, for Version 3.81*. Free Software Foundation.

Stan Development Team. 2018. “RStan: The R Interface to Stan.” <http://mc-stan.org/>.

Stavros, E Natasha, John T Abatzoglou, Donald McKenzie, and Narasimhan K Larkin. 2014. “Regional Projections of the Likelihood of Very Large Wildland Fires Under a Changing Climate in the Contiguous Western United States.” *Climatic Change* 126 (3-4). Springer: 455–68.

Syphard, Alexandra D. AD, Volker C. VC Radeloff, Jon E. Keeley, Todd J. Hawbaker, Murray K. Clayton, Susan I. Stewart, and Roger B. Hammer. 2007. “Human influence on California

fire regimes.” *Ecological Applications* 17 (5): 1388–1402.

Syphard, Alexandra D., Jon E. Keeley, Anne H. Pfaff, and Ken Ferschweiler. 2017. “Human presence diminishes the importance of climate in driving fire activity across the United States.” *Proceedings of the National Academy of Sciences*. doi:10.1073/pnas.1713885114.

Tedim, Fantina, Vittorio Leone, Malik Amraoui, Christophe Bouillon, Michael R Coughlan, Giuseppe M Delogu, Paulo M Fernandes, et al. 2018. “Defining Extreme Wildfire Events: Difficulties, Challenges, and Impacts.” *Fire* 1 (1). Multidisciplinary Digital Publishing Institute: 9.

Tran, Dustin, Matthew D Hoffman, Rif A Saurous, Eugene Brevdo, Kevin Murphy, and David M Blei. 2017. “Deep Probabilistic Programming.” *arXiv Preprint arXiv:1701.03757*.

Vilar, Lara, Douglas G Woolford, David L Martell, and M Pilar Martín. 2010. “A Model for Predicting Human-Caused Wildfire Occurrence in the Region of Madrid, Spain.” *International Journal of Wildland Fire* 19 (3). CSIRO: 325–37.

Westerling, AL, BP Bryant, HK Preisler, TP Holmes, HG Hidalgo, T Das, and SR Shrestha. 2011. “Climate Change and Growth Scenarios for California Wildfire.” *Climatic Change* 109 (1). Springer: 445–63.

Westerling, Anthony LeRoy. 2016. “Increasing Western Us Forest Wildfire Activity: Sensitivity to Changes in the Timing of Spring.” *Phil. Trans. R. Soc. B* 371 (1696). The Royal Society: 20150178.

Wickham, Hadley. 2017a. *Assertthat: Easy Pre and Post Assertions*. <https://CRAN.R-project.org/package=assertthat>.

———. 2017b. *Tidyverse: Easily Install and Load the 'Tidyverse'*. <https://CRAN.R-project.org/package=tidyverse>.

Wiitala, Marc R. 1999. “Assessing the Risk of Cumulative Burned Acreage Using the Poisson Probability Model.” *Fire Economics, Planning, and Policy: Bottom Lines*. Citeseer, 51.

Wilke, Claus O. 2017. *Cowplot: Streamlined Plot Theme and Plot Annotations for 'Ggplot2'*.

<https://CRAN.R-project.org/package=cowplot>.

Williams, Jerry. 2013. “Exploring the Onset of High-Impact Mega-Fires Through a Forest Land Management Prism.” *Forest Ecology and Management* 294. Elsevier: 4–10.

Wood, S.N. 2017. *Generalized Additive Models: An Introduction with R*. 2nd ed. Chapman; Hall/CRC.

Woolford, DG, DR Bellhouse, WJ Braun, Ch B Dean, DL Martell, and J Sun. 2011. “A Spatio-Temporal Model for People-Caused Forest Fire Occurrence in the Romeo Malette Forest.” *Journal of Environmental Statistics* 2: 2–16.

Woolford, Douglas G, CB Dean, David L Martell, Jiguo Cao, and BM Wotton. 2014. “Lightning-Caused Forest Fire Risk in Northwestern Ontario, Canada, Is Increasing and Associated with Anomalies in Fire Weather.” *Environmetrics* 25 (6). Wiley Online Library: 406–16.

Yao, Yuling, Aki Vehtari, Daniel Simpson, Andrew Gelman, and others. 2017. “Using Stacking to Average Bayesian Predictive Distributions.” *Bayesian Analysis*. International Society for Bayesian Analysis.

Zeileis, Achim, and Gabor Grothendieck. 2005. “Zoo: S3 Infrastructure for Regular and Irregular Time Series.” *Journal of Statistical Software* 14 (6): 1–27. doi:10.18637/jss.v014.i06.

Zorzetto, E, G Botter, and M Marani. 2016. “On the Emergence of Rainfall Extremes from Ordinary Events.” *Geophysical Research Letters* 43 (15). Wiley Online Library: 8076–82.

Supporting Information

Prior specifications

Prior distributions were chosen to regularize coefficients on the distribution specific means $\beta^{(\mu)}$ and structural zero parameters $\beta^{(\pi)}$. We used a regularized horseshoe prior on these coefficients, which shrinks irrelevant coefficients towards zero, while regularizing nonzero coefficients (Piiironen, Vehtari, and others 2017). For zero-inflated models, we used a multivariate version of the regularized horseshoe (Peltola et al. 2014):

$$\begin{pmatrix} \beta_j^{(\mu)} \\ \beta_j^{(\pi)} \end{pmatrix} \sim \text{N} \left(\mathbf{0}, \begin{pmatrix} \tau_1^2 \tilde{\lambda}_{1,j}^2 & \rho \tau_1 \tau_2 \tilde{\lambda}_{1,j} \tilde{\lambda}_{2,j} \\ \rho \tau_1 \tau_2 \tilde{\lambda}_{1,j} \tilde{\lambda}_{2,j} & \tau_2^2 \tilde{\lambda}_{2,j}^2 \end{pmatrix} \right),$$

$$\tilde{\lambda}_{m,j}^2 = \frac{c_m^2 \lambda_j^2}{c_m^2 + \tau_m^2 \lambda_j^2},$$

for each response dimension $m = 1, 2$ and coefficient $j = 1, \dots, p$. Here ρ is a correlation parameter, τ_1 and τ_2 are global variance hyperparameters, c_1 and c_2 are hyperparameters that determine the amount of shrinkage on the largest coefficients, and λ_j is a local scale parameter drawn from a half-Cauchy distribution that control the amount of shrinkage applied to coefficient j (Piiironen, Vehtari, and others 2017). With this prior specification, information can be shared across the two response dimensions through the correlation parameter ρ , and/or through the local scale parameters λ_j . For count models without structural zeros (the Poisson and negative binomial models), this multivariate prior simplifies to a univariate regularized horseshoe prior.

Spatiotemporal random effects were constructed using a temporally autoregressive, spatially intrinsically autoregressive formulation (Besag and Kooperberg 1995; Banerjee, Carlin, and Gelfand 2014). Temporarily suppressing the superscript that indicates whether the effects are on μ or π , and denoting column t from an $S \times T$ Φ as ϕ_t we have:

$$\phi_{t=1} \sim \text{N}(\mathbf{0}, (\tau^{(\phi)}(\mathbf{D} - \mathbf{W}))^{-1})$$

$$\phi_t \sim N(\eta\phi_{t-1}, (\tau^{(\phi)}(\mathbf{D} - \mathbf{W}))^{-1}), \quad t = 2, \dots, T$$

where η is a temporal dependence parameter, $\tau^{(\phi)}$ is a precision parameter, \mathbf{D} is an $S \times S$ diagonal matrix with entries corresponding to the number of spatial neighbors for each spatial unit, and \mathbf{W} is an $S \times S$ spatial adjacency matrix with nonzero elements only when spatial unit i is a neighbor of spatial unit j ($w_{i,j} = 1$ if i is a neighbor of j , and $w_{i,j} = 0$ otherwise, including $w_{i,i} = 0$ for all i). $\tau^{(\phi)}$ is a precision parameter. We imposed a soft identifiability constraint that places high prior mass near $\sum_{s=1}^S \phi_{t,s}^* = 0$ for all t .

We applied a univariate regularized horseshoe prior to all β coefficients in burn area models (Piironen, Vehtari, and others 2017):

$$\beta_j \sim N\left(0, \tau^2 \tilde{\lambda}_j^2\right), \quad \tilde{\lambda}_j^2 = \frac{c^2 \lambda_j^2}{c^2 + \tau^2 \lambda_j^2},$$

Spatiotemporal random effects were constructed in the same way as for the count models.

Joint distributions

Here we provide the unnormalized posterior densities for each model. Square brackets represent a probability mass or density function. Parameterizations for model likelihoods are provided first, followed by the factorization of the joint distribution, with explicit priors.

Poisson wildfire count model

We used the following parameterization of the Poisson distribution:

$$[n|\mu] = \frac{\mu^n e^{-\mu}}{n!},$$

where μ is the mean and variance.

The unnormalized posterior density of this model is:

$$\begin{aligned} [\boldsymbol{\beta}^{(\mu)}, \alpha^{(\mu)}, \boldsymbol{\phi}, \sigma^{(\phi)}, \eta, \boldsymbol{\lambda}, c, \tau | \mathbf{N}] \propto & \\ & \prod_{s=1}^S \prod_{t=1}^T [n_{s,t} | \boldsymbol{\beta}^{(\mu)}, \alpha^{(\mu)}, \phi_{s,t}] \times \\ & [\phi_1 | \sigma^{(\phi)}] \prod_{t=2}^T [\phi_t | \phi_{t-1}, \sigma^{(\phi)}, \eta] \times \\ & \prod_{j=1}^p [\beta_j^{(\mu)} | \lambda_j, c, \tau] [\lambda_j] \times \\ & [\sigma^{(\phi)}] [\eta] [c] [\tau] [\alpha^{(\mu)}] \end{aligned}$$

$$\begin{aligned}
 &= \prod_{s=1}^S \prod_{t=1}^T \text{Poisson}(n_{s,t} | \exp(\alpha^{(\mu)} + \mathbf{X}_{(s,t)} \boldsymbol{\beta}^{(\mu)} + \phi_{s,t})) \times \\
 &\quad \text{Normal}(\boldsymbol{\phi}_1 | \mathbf{0}, ((\sigma^{(\phi)})^{-2}(\mathbf{D} - \mathbf{W}))^{-1}) \times \\
 &\quad \prod_{t=2}^T \text{Normal}(\boldsymbol{\phi}_t | \eta \boldsymbol{\phi}_{t-1}, ((\sigma^{(\phi)})^{-2}(\mathbf{D} - \mathbf{W}))^{-1}) \times \\
 &\quad \prod_{j=1}^p \text{Normal}\left(\beta_j^{(\mu)} | 0, \frac{\tau^2 c^2 \lambda_j^2}{c^2 + \tau^2 \lambda_j^2}\right) \times \text{Cauchy}^+(\lambda_j | 0, 1) \times \\
 &\text{Normal}^+(\sigma^{(\phi)} | 0, 1^2) \times \text{Beta}(\eta | 1, 1) \times \text{Inv-Gamma}(c^2 | 2.5, 10) \times \\
 &\quad \text{Normal}^+(\tau | 0, 5^2) \times \text{Normal}(\alpha^{(\mu)} | 0, 5^2).
 \end{aligned}$$

Negative binomial wildfire count model

We used the following parameterization of the negative binomial distribution:

$$[n|\mu, \delta] = \binom{n + \delta - 1}{n} \left(\frac{\mu}{\mu + \delta}\right)^n \left(\frac{\delta}{\mu + \delta}\right)^\delta,$$

where μ is the mean, and δ is a dispersion parameter.

The unnormalized posterior density of this model is:

$$\begin{aligned} [\boldsymbol{\beta}^{(\mu)}, \boldsymbol{\alpha}^{(\mu)}, \boldsymbol{\phi}, \sigma^{(\phi)}, \eta, \boldsymbol{\lambda}, c, \tau, \delta \mid \mathbf{N}] &\propto \\ &\prod_{s=1}^S \prod_{t=1}^T [n_{s,t} | \boldsymbol{\beta}^{(\mu)}, \boldsymbol{\alpha}^{(\mu)}, \phi_{s,t}, \delta] \times \\ &[\boldsymbol{\phi}_1 | \sigma^{(\phi)}] \prod_{t=2}^T [\boldsymbol{\phi}_t | \boldsymbol{\phi}_{t-1}, \sigma^{(\phi)}, \eta] \times \\ &\prod_{j=1}^p [\beta_j^{(\mu)} | \lambda_j, c, \tau] [\lambda_j] \times \\ &[\sigma^{(\phi)}] [\eta] [c] [\tau] [\boldsymbol{\alpha}^{(\mu)}] [\delta] \end{aligned}$$

$$\begin{aligned} &= \prod_{s=1}^S \prod_{t=1}^T \text{Negative Binomial}(n_{s,t} | \exp(\boldsymbol{\alpha}^{(\mu)} + \mathbf{X}_{(s,t)} \boldsymbol{\beta}^{(\mu)} + \phi_{s,t}), \delta) \times \\ &\quad \text{Normal}(\boldsymbol{\phi}_1 | \mathbf{0}, ((\sigma^{(\phi)})^{-2} (\mathbf{D} - \mathbf{W}))^{-1}) \times \\ &\quad \prod_{t=2}^T \text{Normal}(\boldsymbol{\phi}_t | \eta \boldsymbol{\phi}_{t-1}, ((\sigma^{(\phi)})^{-2} (\mathbf{D} - \mathbf{W}))^{-1}) \times \\ &\quad \prod_{j=1}^p \text{Normal}\left(\beta_j^{(\mu)} | 0, \frac{\tau^2 c^2 \lambda_j^2}{c^2 + \tau^2 \lambda_j^2}\right) \times \text{Cauchy}^+(\lambda_j | 0, 1) \times \\ &\quad \text{Normal}^+(\sigma^{(\phi)} | 0, 1^2) \times \text{Beta}(\eta | 1, 1) \times \text{Inv-Gamma}(c^2 | 2.5, 10) \times \\ &\quad \text{Normal}^+(\tau | 0, 5^2) \times \text{Normal}(\boldsymbol{\alpha}^{(\mu)} | 0, 5^2) \times \text{Normal}^+(\delta | 0, 5^2). \end{aligned}$$

Zero-inflated Poisson wildfire count model

We used the following parameterization of the zero-inflated Poisson distribution:

$$[n|\mu, \pi] = I_{n=0}(1 - \pi + \pi e^{-\mu}) + I_{n>0}\pi \frac{\mu^n e^{-\mu}}{n!},$$

where μ is the Poisson mean, and $1 - \pi$ is the probability of an extra zero.

The unnormalized posterior density of this model is:

$$\begin{aligned} & [\boldsymbol{\beta}^{(\mu)}, \alpha^{(\mu)}, \boldsymbol{\beta}^{(\pi)}, \alpha^{(\pi)}, \boldsymbol{\phi}^{(\mu)}, \sigma^{(\phi, \mu)}, \eta^{(\mu)}, \boldsymbol{\phi}^{(\pi)}, \sigma^{(\phi, \pi)}, \eta^{(\pi)}, \boldsymbol{\lambda}, c, \tau, \rho \mid \mathbf{N}] \propto \\ & \prod_{s=1}^S \prod_{t=1}^T [n_{s,t} | \boldsymbol{\beta}^{(\mu)}, \alpha^{(\mu)}, \boldsymbol{\beta}^{(\pi)}, \alpha^{(\pi)}, \phi_{s,t}^{(\mu)}, \phi_{s,t}^{(\pi)}] \times \\ & [\phi_1^{(\mu)} | \sigma^{(\phi, \mu)}] \prod_{t=2}^T [\phi_t^{(\mu)} | \phi_{t-1}^{(\mu)}, \sigma^{(\phi, \mu)}, \eta^{(\mu)}] \times \\ & [\phi_1^{(\pi)} | \sigma^{(\phi, \pi)}] \prod_{t=2}^T [\phi_t^{(\pi)} | \phi_{t-1}^{(\pi)}, \sigma^{(\phi, \pi)}, \eta^{(\pi)}] \times \\ & \prod_{j=1}^p [\beta_j^{(\mu)}, \beta_j^{(\pi)} | \lambda_j, c, \tau, \rho] [\lambda_j] \times \\ & [\sigma^{(\phi, \mu)}] [\sigma^{(\phi, \pi)}] [\eta^{(\mu)}] [\eta^{(\pi)}] [\alpha^{(\mu)}] [\alpha^{(\pi)}] [\rho] \prod_{m=1}^2 [c_m] [\tau_m] \end{aligned}$$

$$\begin{aligned}
&= \prod_{s=1}^S \prod_{t=1}^T \text{ZIP}(n_{s,t} | e^{\alpha^{(\mu)} + \mathbf{X}_{(s,t)} \boldsymbol{\beta}^{(\mu)} + \phi_{s,t}^{(\mu)}}, \text{logit}^{-1}(\alpha^{(\pi)} + \mathbf{X}_{(s,t)} \boldsymbol{\beta}^{(\pi)} + \phi_{s,t}^{(\pi)})) \times \\
&\quad \text{Normal}(\boldsymbol{\phi}_1^{(\mu)} | \mathbf{0}, ((\sigma^{(\phi, \mu)})^{-2}(\mathbf{D} - \mathbf{W}))^{-1}) \times \\
&\quad \prod_{t=2}^T \text{Normal}(\boldsymbol{\phi}_t^{(\mu)} | \eta^{(\mu)} \boldsymbol{\phi}_{t-1}^{(\mu)}, ((\sigma^{(\phi, \mu)})^{-2}(\mathbf{D} - \mathbf{W}))^{-1}) \times \\
&\quad \text{Normal}(\boldsymbol{\phi}_1^{(\pi)} | \mathbf{0}, ((\sigma^{(\phi, \pi)})^{-2}(\mathbf{D} - \mathbf{W}))^{-1}) \times \\
&\quad \prod_{t=2}^T \text{Normal}(\boldsymbol{\phi}_t^{(\pi)} | \eta^{(\pi)} \boldsymbol{\phi}_{t-1}^{(\pi)}, ((\sigma^{(\phi, \pi)})^{-2}(\mathbf{D} - \mathbf{W}))^{-1}) \times \\
&\quad \prod_{j=1}^p \text{N} \left(\begin{pmatrix} \beta_j^{(\mu)} \\ \beta_j^{(\pi)} \end{pmatrix} \middle| \mathbf{0}, \begin{pmatrix} \tau_1^2 \frac{c_1^2 \lambda_j^2}{c_1^2 + \tau_1^2 \lambda_j^2} & \rho \tau_1 \tau_2 \sqrt{\frac{c_1^2 \lambda_j^2}{c_1^2 + \tau_1^2 \lambda_j^2}} \sqrt{\frac{c_2^2 \lambda_j^2}{c_2^2 + \tau_2^2 \lambda_j^2}} \\ \rho \tau_1 \tau_2 \sqrt{\frac{c_1^2 \lambda_j^2}{c_1^2 + \tau_1^2 \lambda_j^2}} \sqrt{\frac{c_2^2 \lambda_j^2}{c_2^2 + \tau_2^2 \lambda_j^2}} & \tau_2^2 \frac{c_2^2 \lambda_j^2}{c_2^2 + \tau_2^2 \lambda_j^2} \end{pmatrix} \right) \times \\
&\quad \prod_{j=1}^p \text{Cauchy}^+(\lambda_j | 0, 1) \times \\
&\quad \text{Normal}^+(\sigma^{(\phi, \mu)} | 0, 1^2) \times \text{Normal}^+(\sigma^{(\phi, \pi)} | 0, 1^2) \times \\
&\quad \text{Beta}(\eta^{(\mu)} | 1, 1) \times \text{Beta}(\eta^{(\pi)} | 1, 1) \times \\
&\quad \text{Normal}(\alpha^{(\mu)} | 0, 5^2) \times \text{Normal}(\alpha^{(\pi)} | 0, 5^2) \times \text{LKJ}(\rho | 3) \times \\
&\quad \prod_{m=1}^2 \text{Inv-Gamma}(c_m^2 | 2.5, 10) \times \text{Normal}^+(\tau_m | 0, 5^2).
\end{aligned}$$

Zero-inflated negative binomial wildfire count model

We used the following parameterization of the zero-inflated negative binomial distribution:

$$[n|\mu, \delta, \pi] = I_{n=0}(1 - \pi + \pi\left(\frac{\delta}{\mu + \delta}\right)^\delta) + I_{n>0}\binom{n + \delta - 1}{n}\left(\frac{\mu}{\mu + \delta}\right)^n\left(\frac{\delta}{\mu + \delta}\right)^\delta,$$

where μ is the negative binomial mean, δ is the negative binomial dispersion, and π is the probability of an extra zero.

The unnormalized posterior density of this model is:

$$\begin{aligned} & [\boldsymbol{\beta}^{(\mu)}, \alpha^{(\mu)}, \boldsymbol{\beta}^{(\pi)}, \alpha^{(\pi)}, \boldsymbol{\phi}^{(\mu)}, \sigma^{(\phi, \mu)}, \boldsymbol{\eta}^{(\mu)}, \boldsymbol{\phi}^{(\pi)}, \sigma^{(\phi, \pi)}, \boldsymbol{\eta}^{(\pi)}, \boldsymbol{\lambda}, c, \tau, \rho, \delta | \mathbf{N}] \propto \\ & \prod_{s=1}^S \prod_{t=1}^T [n_{s,t} | \boldsymbol{\beta}^{(\mu)}, \alpha^{(\mu)}, \boldsymbol{\beta}^{(\pi)}, \alpha^{(\pi)}, \phi_{s,t}^{(\mu)}, \phi_{s,t}^{(\pi)}, \delta] \times \\ & [\phi_1^{(\mu)} | \sigma^{(\phi, \mu)}] \prod_{t=2}^T [\phi_t^{(\mu)} | \phi_{t-1}^{(\mu)}, \sigma^{(\phi, \mu)}, \boldsymbol{\eta}^{(\mu)}] \times \\ & [\phi_1^{(\pi)} | \sigma^{(\phi, \pi)}] \prod_{t=2}^T [\phi_t^{(\pi)} | \phi_{t-1}^{(\pi)}, \sigma^{(\phi, \pi)}, \boldsymbol{\eta}^{(\pi)}] \times \\ & \prod_{j=1}^p [\beta_j^{(\mu)}, \beta_j^{(\pi)} | \lambda_j, c, \tau, \rho] [\lambda_j] \times \\ & [\sigma^{(\phi, \mu)}] [\sigma^{(\phi, \pi)}] [\boldsymbol{\eta}^{(\mu)}] [\boldsymbol{\eta}^{(\pi)}] [\alpha^{(\mu)}] [\alpha^{(\pi)}] [\rho] [\delta] \prod_{m=1}^2 [c_m] [\tau_m]. \end{aligned}$$

$$\begin{aligned}
&= \prod_{s=1}^S \prod_{t=1}^T \text{ZINB}(n_{s,t} | e^{\alpha^{(\mu)} + \mathbf{X}_{(s,t)} \boldsymbol{\beta}^{(\mu)} + \phi_{s,t}^{(\mu)}}, \delta, \text{logit}^{-1}(\alpha^{(\pi)} + \mathbf{X}_{(s,t)} \boldsymbol{\beta}^{(\pi)} + \phi_{s,t}^{(\pi)})) \times \\
&\quad \text{Normal}(\boldsymbol{\phi}_1^{(\mu)} | \mathbf{0}, ((\sigma^{(\phi, \mu)})^{-2}(\mathbf{D} - \mathbf{W}))^{-1}) \times \\
&\quad \prod_{t=2}^T \text{Normal}(\boldsymbol{\phi}_t^{(\mu)} | \eta^{(\mu)} \boldsymbol{\phi}_{t-1}^{(\mu)}, ((\sigma^{(\phi, \mu)})^{-2}(\mathbf{D} - \mathbf{W}))^{-1}) \times \\
&\quad \text{Normal}(\boldsymbol{\phi}_1^{(\pi)} | \mathbf{0}, ((\sigma^{(\phi, \pi)})^{-2}(\mathbf{D} - \mathbf{W}))^{-1}) \times \\
&\quad \prod_{t=2}^T \text{Normal}(\boldsymbol{\phi}_t^{(\pi)} | \eta^{(\pi)} \boldsymbol{\phi}_{t-1}^{(\pi)}, ((\sigma^{(\phi, \pi)})^{-2}(\mathbf{D} - \mathbf{W}))^{-1}) \times \\
&\quad \prod_{j=1}^p \text{N} \left(\begin{pmatrix} \beta_j^{(\mu)} \\ \beta_j^{(\pi)} \end{pmatrix} \middle| \mathbf{0}, \begin{pmatrix} \tau_1^2 \frac{c_1^2 \lambda_j^2}{c_1^2 + \tau_1^2 \lambda_j^2} & \rho \tau_1 \tau_2 \sqrt{\frac{c_1^2 \lambda_j^2}{c_1^2 + \tau_1^2 \lambda_j^2}} \sqrt{\frac{c_2^2 \lambda_j^2}{c_2^2 + \tau_2^2 \lambda_j^2}} \\ \rho \tau_1 \tau_2 \sqrt{\frac{c_1^2 \lambda_j^2}{c_1^2 + \tau_1^2 \lambda_j^2}} \sqrt{\frac{c_2^2 \lambda_j^2}{c_2^2 + \tau_2^2 \lambda_j^2}} & \tau_2^2 \frac{c_2^2 \lambda_j^2}{c_2^2 + \tau_2^2 \lambda_j^2} \end{pmatrix} \right) \times \\
&\quad \prod_{j=1}^p \text{Cauchy}^+(\lambda_j | 0, 1) \times \\
&\quad \text{Normal}^+(\sigma^{(\phi, \mu)} | 0, 1^2) \times \text{Normal}^+(\sigma^{(\phi, \pi)} | 0, 1^2) \times \\
&\quad \text{Beta}(\eta^{(\mu)} | 1, 1) \times \text{Beta}(\eta^{(\pi)} | 1, 1) \times \\
&\quad \text{Normal}(\alpha^{(\mu)} | 0, 5^2) \times \text{Normal}(\alpha^{(\pi)} | 0, 5^2) \times \text{LKJ}(\rho | 3) \times \text{Normal}^+(\delta | 0, 5^2) \times \\
&\quad \prod_{m=1}^2 \text{Inv-Gamma}(c_m^2 | 2.5, 10) \times \text{Normal}^+(\tau_m | 0, 5^2).
\end{aligned}$$

Generalized Pareto/Lomax burn area model

We used the following parameterization of the GPD/Lomax distribution:

$$[y|\sigma, \kappa] = \frac{1}{\sigma} \left(\frac{\kappa y}{\sigma} + 1 \right)^{-(\kappa+1)\kappa^{-1}},$$

where κ is a shape parameter and σ is a scale parameter.

The unnormalized posterior density of this model is:

$$\begin{aligned} [\boldsymbol{\beta}, \alpha, \boldsymbol{\phi}, \sigma^{(\phi)}, \eta, \kappa^{(L)}, \boldsymbol{\lambda}, c, \tau | \mathbf{y}] &\propto \\ &\prod_{i=1}^{n_{\text{tot}}} [y_i | \boldsymbol{\beta}, \alpha, \phi_{s_i, t_i}, \kappa^{(L)}] \times \\ &[\boldsymbol{\phi}_1 | \sigma^{(\phi)}] \prod_{t=2}^T [\boldsymbol{\phi}_t | \boldsymbol{\phi}_{t-1}, \sigma^{(\phi)}, \eta] \times \\ &\prod_{j=1}^p [\beta_j | \lambda_j, c, \tau] [\lambda_j] \times \\ &[\alpha][c][\tau][\kappa^{(L)}][\eta][\sigma^{(\phi)}] \\ &= \prod_{i=1}^{n_{\text{tot}}} \text{Lomax}(y_i | \kappa^{(L)}, e^{\alpha + \mathbf{X}_{(s_i, t_i)} \boldsymbol{\beta} + \phi_{s_i, t_i}}) \times \\ &\text{Normal}(\boldsymbol{\phi}_1 | \mathbf{0}, ((\sigma^{(\phi)})^{-2}(\mathbf{D} - \mathbf{W}))^{-1}) \times \\ &\prod_{t=2}^T \text{Normal}(\boldsymbol{\phi}_t | \eta \boldsymbol{\phi}_{t-1}, ((\sigma^{(\phi)})^{-2}(\mathbf{D} - \mathbf{W}))^{-1}) \times \\ &\prod_{j=1}^p \text{Normal}\left(\beta_j | 0, \frac{\tau^2 c^2 \lambda_j^2}{c^2 + \tau^2 \lambda_j^2}\right) \times \text{Cauchy}^+(\lambda_j | 0, 1) \times \\ &\text{Normal}(\alpha | 0, 5^2) \times \text{Inv-Gamma}(c^2 | 2.5, 10) \times \text{Normal}^+(\tau | 0, 5^2) \\ &\text{Normal}^+(\kappa^{(L)} | 0, 5^2) \times \text{Beta}(\eta | 1, 1) \times \text{Normal}^+(\sigma^{(\phi)} | 0, 1^2). \end{aligned}$$

Tapered Pareto burn area model

We used the following parameterization of the tapered Pareto distribution:

$$[y|\kappa, \nu] = \left(\frac{\kappa}{y} + \frac{1}{\nu}\right) \exp(-x/\nu),$$

where κ is a shape parameter and ν a taper parameter.

The unnormalized posterior density of this model is:

$$\begin{aligned} [\boldsymbol{\beta}, \alpha, \boldsymbol{\phi}, \sigma^{(\phi)}, \eta, \nu, \boldsymbol{\lambda}, c, \tau | \mathbf{y}] &\propto \\ &\prod_{i=1}^{n_{\text{tot}}} [y_i | \boldsymbol{\beta}, \alpha, \phi_{s_i, t_i}, \nu] \times \\ &[\boldsymbol{\phi}_1 | \sigma^{(\phi)}] \prod_{t=2}^T [\boldsymbol{\phi}_t | \boldsymbol{\phi}_{t-1}, \sigma^{(\phi)}, \eta] \times \\ &\prod_{j=1}^p [\beta_j | \lambda_j, c, \tau] [\lambda_j] \times \\ &[\alpha][c][\tau][\nu][\eta][\sigma^{(\phi)}] \\ &= \prod_{i=1}^{n_{\text{tot}}} \text{Tapered Pareto}(y_i | e^{\alpha + \mathbf{X}_{(s_i, t_i)} \boldsymbol{\beta} + \phi_{s_i, t_i}}, \nu) \times \\ &\quad \text{Normal}(\boldsymbol{\phi}_1 | \mathbf{0}, ((\sigma^{(\phi)})^{-2}(\mathbf{D} - \mathbf{W}))^{-1}) \times \\ &\quad \prod_{t=2}^T \text{Normal}(\boldsymbol{\phi}_t | \eta \boldsymbol{\phi}_{t-1}, ((\sigma^{(\phi)})^{-2}(\mathbf{D} - \mathbf{W}))^{-1}) \times \\ &\quad \prod_{j=1}^p \text{Normal}\left(\beta_j | 0, \frac{\tau^2 c^2 \lambda_j^2}{c^2 + \tau^2 \lambda_j^2}\right) \times \text{Cauchy}^+(\lambda_j | 0, 1) \times \\ &\quad \text{Normal}(\alpha | 0, 5^2) \times \text{Inv-Gamma}(c^2 | 2.5, 10) \times \text{Normal}^+(\tau | 0, 5^2) \times \\ &\quad \text{Cauchy}^+(\nu | 0, 1) \times \text{Beta}(\eta | 1, 1) \times \text{Normal}^+(\sigma^{(\phi)} | 0, 1^2). \end{aligned}$$

Lognormal burn area model

We used the following parameterization of the lognormal distribution:

$$[y|\mu, \sigma] = \frac{1}{y} \frac{1}{\sigma\sqrt{2\pi}} \exp\left(-\frac{(\log(y) - \mu)^2}{2\sigma^2}\right),$$

where μ and σ are location and scale parameters, respectively.

The unnormalized posterior density of this model is:

$$\begin{aligned} [\boldsymbol{\beta}, \alpha, \boldsymbol{\phi}, \sigma^{(\phi)}, \eta, \sigma, \boldsymbol{\lambda}, c, \tau | \mathbf{y}] &\propto \\ &\prod_{i=1}^{n_{\text{tot}}} [y_i | \beta, \alpha, \phi_{s_i, t_i}, \sigma] \times \\ &[\boldsymbol{\phi}_1 | \sigma^{(\phi)}] \prod_{t=2}^T [\boldsymbol{\phi}_t | \boldsymbol{\phi}_{t-1}, \sigma^{(\phi)}, \eta] \times \\ &\prod_{j=1}^p [\beta_j | \lambda_j, c, \tau] [\lambda_j] \times \\ &[\alpha][c][\tau][\sigma][\eta][\sigma^{(\phi)}] \\ &= \prod_{i=1}^{n_{\text{tot}}} \text{Lognormal}(y_i | \alpha + \mathbf{X}_{(s_i, t_i)} \boldsymbol{\beta} + \phi_{s_i, t_i}, \sigma) \times \\ &\quad \text{Normal}(\boldsymbol{\phi}_1 | \mathbf{0}, ((\sigma^{(\phi)})^{-2}(\mathbf{D} - \mathbf{W}))^{-1}) \times \\ &\quad \prod_{t=2}^T \text{Normal}(\boldsymbol{\phi}_t | \eta \boldsymbol{\phi}_{t-1}, ((\sigma^{(\phi)})^{-2}(\mathbf{D} - \mathbf{W}))^{-1}) \times \\ &\quad \prod_{j=1}^p \text{Normal}\left(\beta_j | 0, \frac{\tau^2 c^2 \lambda_j^2}{c^2 + \tau^2 \lambda_j^2}\right) \times \text{Cauchy}^+(\lambda_j | 0, 1) \times \\ &\quad \text{Normal}(\alpha | 0, 5^2) \times \text{Inv-Gamma}(c^2 | 2.5, 10) \times \text{Normal}^+(\tau | 0, 5^2) \times \\ &\quad \text{Normal}^+(\sigma | 0, 5^2) \times \text{Beta}(\eta | 1, 1) \times \text{Normal}^+(\sigma^{(\phi)} | 0, 1^2). \end{aligned}$$

Gamma burn area model

We used the following parameterization of the gamma distribution:

$$[y|\kappa, \sigma] = \frac{1}{\Gamma(\kappa)\sigma^\kappa} y^{\kappa-1} \exp(-y/\sigma),$$

where κ is a shape parameter and σ a scale parameter.

The unnormalized posterior density of this model is:

$$\begin{aligned} & [\boldsymbol{\beta}, \alpha, \boldsymbol{\phi}, \sigma^{(\phi)}, \eta, \kappa, \boldsymbol{\lambda}, c, \tau | \mathbf{y}] \propto \\ & \prod_{i=1}^{n_{\text{tot}}} [y_i | \beta, \alpha, \phi_{s_i, t_i}, \kappa] \times \\ & [\boldsymbol{\phi}_1 | \sigma^{(\phi)}] \prod_{t=2}^T [\boldsymbol{\phi}_t | \boldsymbol{\phi}_{t-1}, \sigma^{(\phi)}, \eta] \times \\ & \prod_{j=1}^p [\beta_j | \lambda_j, c, \tau] [\lambda_j] \times \\ & [\alpha] [c] [\tau] [\kappa] [\eta] [\sigma^{(\phi)}] \\ & = \prod_{i=1}^{n_{\text{tot}}} \text{Gamma}(y_i | \kappa, \kappa / \exp(\alpha + \mathbf{X}_{(s_i, t_i)} \boldsymbol{\beta} + \phi_{s_i, t_i})) \times \\ & \quad \text{Normal}(\boldsymbol{\phi}_1 | \mathbf{0}, ((\sigma^{(\phi)})^{-2} (\mathbf{D} - \mathbf{W}))^{-1}) \times \\ & \quad \prod_{t=2}^T \text{Normal}(\boldsymbol{\phi}_t | \eta \boldsymbol{\phi}_{t-1}, ((\sigma^{(\phi)})^{-2} (\mathbf{D} - \mathbf{W}))^{-1}) \times \\ & \quad \prod_{j=1}^p \text{Normal}\left(\beta_j | 0, \frac{\tau^2 c^2 \lambda_j^2}{c^2 + \tau^2 \lambda_j^2}\right) \times \text{Cauchy}^+(\lambda_j | 0, 1) \times \\ & \quad \text{Normal}(\alpha | 0, 5^2) \times \text{Inv-Gamma}(c^2 | 2.5, 10) \times \text{Normal}^+(\tau | 0, 5^2) \times \\ & \quad \text{Normal}^+(\kappa | 0, 5^2) \times \text{Beta}(\eta | 1, 1) \times \text{Normal}^+(\sigma^{(\phi)} | 0, 1^2). \end{aligned}$$

Weibull burn area model

We used the following parameterization of the Weibull distribution:

$$[y|\kappa, \sigma] = \frac{\kappa}{\sigma} \left(\frac{y}{\sigma}\right)^{\kappa-1} \exp\left(-\left(\frac{y}{\sigma}\right)^\kappa\right),$$

where κ is a shape parameter and σ is a scale parameter.

The unnormalized posterior density of this model is:

$$\begin{aligned} [\boldsymbol{\beta}, \alpha, \boldsymbol{\phi}, \sigma^{(\phi)}, \eta, \kappa, \lambda, c, \tau | \mathbf{y}] &\propto \\ &\prod_{i=1}^{n_{\text{tot}}} [y_i | \beta, \alpha, \phi_{s_i, t_i}, \kappa] \times \\ &[\boldsymbol{\phi}_1 | \sigma^{(\phi)}] \prod_{t=2}^T [\boldsymbol{\phi}_t | \boldsymbol{\phi}_{t-1}, \sigma^{(\phi)}, \eta] \times \\ &\prod_{j=1}^p [\beta_j | \lambda_j, c, \tau] [\lambda_j] \times \\ &[\alpha] [c] [\tau] [\kappa] [\eta] [\sigma^{(\phi)}] \\ &= \prod_{i=1}^{n_{\text{tot}}} \text{Weibull}(y_i | \kappa, \exp(\alpha + \mathbf{X}_{(s_i, t_i)} \boldsymbol{\beta} + \phi_{s_i, t_i})) \times \\ &\quad \text{Normal}(\boldsymbol{\phi}_1 | \mathbf{0}, ((\sigma^{(\phi)})^{-2} (\mathbf{D} - \mathbf{W}))^{-1}) \times \\ &\quad \prod_{t=2}^T \text{Normal}(\boldsymbol{\phi}_t | \eta \boldsymbol{\phi}_{t-1}, ((\sigma^{(\phi)})^{-2} (\mathbf{D} - \mathbf{W}))^{-1}) \times \\ &\quad \prod_{j=1}^p \text{Normal}\left(\beta_j | 0, \frac{\tau^2 c^2 \lambda_j^2}{c^2 + \tau^2 \lambda_j^2}\right) \times \text{Cauchy}^+(\lambda_j | 0, 1) \times \\ &\quad \text{Normal}(\alpha | 0, 5^2) \times \text{Inv-Gamma}(c^2 | 2.5, 10) \times \text{Normal}^+(\tau | 0, 5^2) \times \\ &\quad \text{Normal}^+(\kappa | 0, 5^2) \times \text{Beta}(\eta | 1, 1) \times \text{Normal}^+(\sigma^{(\phi)} | 0, 1^2). \end{aligned}$$